https://doi.org/10.5194/egusphere-2025-2384
Preprint. Discussion started: 26 June 2025

Alongshore Varying Dune Retreat at a Barrier Island

Ronaldyn Dabu[1], Dano Roelvink[1,2], Juan Garzon[3], Ap van Dongeren[1,2]

[1]Coastal and Urban Risk and Resilience, IHE Delft Institute for Water Education, Delft, 2611 AX, The Netherlands

[2]Applied Morphodynamics, Deltares, Delft, 2629 HV, The Netherlands

[3]CIMA, Centre of Marine and Environmental Research\ARNET - Infrastructure Network in Aquatic Research, University of Algarve, Campus de Gambelas, 8000-139, Faro, Portugal

Correspondence to: Ronaldyn Dabu (ronaldyn.e.dabu@gmail.com)

Abstract. Barrier islands often exhibit spatially uneven morphological change due to alongshore variations in wave exposure, sediment supply, and dune morphology, which are influenced by both long-term evolution and short-term storm impacts. We investigate the alongshore variability of shoreline and dune evolution on Culatra Island (Ria Formosa, S. Portugal) over a two-year period (Nov 2009–Nov 2011) encompassing 31 storm events. A coupled modeling framework was developed, combining the one-line ShorelineS coastline model with an impact-based dune erosion and recovery module. The model was forced with hourly offshore wave data from the ERA5 reanalysis (corrected for biases in wave height, direction and period using Faro buoy observations) and transformed to the nearshore with the unstructured-grid SnapWave model. In situ LiDAR surveys and satellite-derived shorelines and dune vegetation lines (using Normalized Difference Vegetation Index (NDVI)) were used for calibration and validation. Model results show that longshore sediment transport gradients dominated shoreline change across most of the island, with net erosion in the sediment-starved western sector and net accretion in the eastern sector. Notably, an erosion "hotspot" in the central-west (transects T42–77) experienced intense storm-induced dune retreat, which supplied sand to the adjacent beach and caused local shoreline advance counter to the regional trend. Overwash at the eastern end contributed to the accretion aligned with the regional trend. The dune module's performance was sensitive to its calibration: a higher wave impact coefficient Cs led to greater dune erosion, while coarse sand d50 and low winds markedly reduced modeled post-storm dune recovery. Model validation using satellite-derived shoreline and dune positions employed R^2 and Pearson correlation metrics, revealing moderate shoreline performance and weaker dune agreement—though general retreat trends were captured across several transects. A correlation analysis indicates that cumulative cross-shore sediment flux (corr = 0.73) and storm duration (corr = 0.48) exert the strongest control on dune retreat whereas peak storm wave direction and initial berm width had minimal influence. Overall, the coupled model captured the observed pattern of alongshore-varying coastal response – including the emergence of a dune erosion hotspot – highlighting the importance of cross-shore sediment exchanges in barrier island evolution and providing useful insights for coastal management of dune systems.

https://doi.org/10.5194/egusphere-2025-2384
Preprint. Discussion started: 26 June 2025

1 Introduction

Barrier islands exhibit significant alongshore variability in their morphodynamic responses to ocean forcing, driven by both natural processes and human interventions. Longshore sediment transport plays a key role: gradients in alongshore transport can produce localized zones of erosion and accretion, especially when the shoreline orientation or wave climate varies along the island's length (Ashton & Murray, 2006). Human structures such as seawalls, groins, and jetties further disrupt sediment pathways, often causing updrift beach accretion and downdrift erosion by blocking or redirecting the longshore sand flux (Masselink & Lazarus, 2019). In addition, sediment exchange at tidal inlets contributes to alongshore differences in sediment supply: ebb-tidal deltas can store sand and periodically release it to adjacent shores via bypassing, so barrier island segments near inlets may experience enhanced accretion or erosion depending on inlet dynamics (FitzGerald et al., 1982; Beck & Wang, 2019; Herrling & Winter, 2018). Collectively, these factors impose pronounced alongshore variability in barrier island behavior, as some sections prograde or remain stable while others recede under the same regional forcing (Bamunawala et al., 2023; Anthony, 2015).

Episodic storm events impose an additional layer of complexity on this alongshore variability. In particular, clusters of storms arriving in close succession can lead to rapid and uneven dune erosion along a barrier island. When multiple storm impacts occur before the beach-dune system recovers, the cumulative effect can exceed that of a single equivalent storm, stripping away dune volume incrementally and expanding erosional hotspots (Dissanayake et al., 2015; van Wiechen et al., 2023). Dune erosion during a storm depends on extreme water levels and wave energy. However, the spatial pattern of dune retreat can vary widely alongshore as a function of pre-storm morphology and the history of preceding storms (Houser, 2013; Beuzen et al., 2019). Thus, a section of coast fronted by a narrower beach or lower dune may suffer disproportionate erosion under sequential storms, whereas more robust sections better withstand initial events only to erode in later events once their sediment buffer is depleted (Dissanayake et al., 2015; Houser, 2013; Beuzen et al., 2019). These clustered-storm impacts effectively compound the inherent variability set by longshore processes, making it challenging to predict coastal evolution without accounting for both alongshore sediment gradients and the timing of extreme events.

Modeling the interplay of long-term alongshore processes and short-term storm-induced changes is difficult, in large part due to uncertainties in the boundary conditions that drive these processes. Coastal evolution models rely on wave and water level inputs that are often derived from hindcasts or reanalysis datasets (e.g., ERA5 wave climate), which carry biases and uncertainties, especially in nearshore regions (Hersbach et al., 2020; Camus et al., 2017). For example, errors in offshore wave direction or over/under-estimation of wave height in a reanalysis can translate into incorrect longshore transport rates and storm erosion predictions at the coast (Stopa & Cheung, 2014; Vousdoukas et al., 2018). This means that even with a perfect process-based model, uncertain boundary conditions can lead to divergent outcomes for shoreline change over decades or dune

https://doi.org/10.5194/egusphere-2025-2384
Preprint. Discussion started: 26 June 2025

retreat in a single storm. Studies such as Fanti et al., 2023 analyzed global buoys and compared them to ERA5 reanalysis for wave heights, directions and periods. Linear regression and bias correction showed improvement in the reanalysis data.

In this study, we address these challenges by employing a simplified one-line shoreline model coupled with a storm-induced dune erosion module, together with a fast unstructured wave propagation model to provide improved nearshore wave forcing. The one-line shoreline model predicts planform coastline change due to gradients in longshore sediment transport, an approach that has proven effective for simulating decadal-scale shoreline evolution on sandy coasts (Ashton & Murray, 2006; Vitousek et al., 2017). We augment this with a dune foot change component that moves wind-blown sand towards the dune and episodically removes sand from the subaerial profile during extreme events, thereby capturing the cross-shore retreat of the dune toe during storms (Larson et al., 2016). To drive both the longshore and cross-shore processes, we use an unstructured spectral wave model ("SnapWave") that rapidly transforms offshore wave conditions to detailed nearshore wave parameters at each alongshore model segment. This wave model accounts for shoaling, refraction and dissipation of directionally spread waves over complex bathymetry (Roelvink et al., 2025). By integrating these components, our modeling framework can simulate the alongshore-variable shoreline changes of a barrier island while also capturing episodic dune impacts from storms, all within a computationally efficient scheme suitable for both large-scale and long-term hindcasts.

Model validation and analysis leverage satellite-derived observations of coastal vegetation as a proxy for dune position and health. We use in situ and remotely sensed data, in particular Normalized Difference Vegetation Index (NDVI) time series from high-resolution satellite imagery, to evaluate model performance in reproducing observed dune retreat and recovery patterns. NDVI correlates with dune vegetation density, offering a spatially continuous indicator of dune erosion or accretion across the study area. This approach aligns with recent developments in open-source tools such as VedgeSat, which automates the extraction of coastal vegetation edges using satellite data to monitor shoreline and dune dynamics (Muir et al., 2024). By comparing model-predicted shoreline and dune toe positions against shore and vegetation lines detected in satellite images, we take advantage of the rich spatial detail and frequency of satellite data for validation. This is particularly valuable in systems like Ria Formosa, where long-term aerial imagery and morphological mapping have revealed strong links between vegetation boundaries and barrier evolution (Kombiadou et al., 2019). This combination provides a robust test of the model's skill in capturing alongshore variability: where the model simulates erosion, a corresponding landward shift or loss of vegetated dune area is expected in the NDVI maps. The combination of modeling and satellite analysis yields both quantitative and qualitative insights into barrier island response over the study period.

Building on this framework, the specific objectives of this study are to: (i) simulate the spatial variability of shoreline change along Culatra over multiple storms using a one-line model calibrated with spatially varying profile parameters; (ii) determine how episodic dune erosion contributes to shoreline advance or retreat in different sectors during storm events; (iii) correct the wave boundary conditions from ERA5 using Faro buoy measurements; (iv) assess model sensitivity to key dune parameters

https://doi.org/10.5194/egusphere-2025-2384
Preprint. Discussion started: 26 June 2025

(particularly the wave impact coefficient *Cs* and sand grain size *d50* that control erosion and recovery); (v) validate modeled shoreline and dune positions against LiDAR and satellite-derived observations, including the use of NDVI (vegetation index) as a proxy for the dune foot position; and (vi) analyze the relationship between dune retreat and storm characteristics (e.g. wave height, storm duration, peak wave angle, runup, initial berm width, cumulative dune erosion during storms)

2 Study Area

Culatra Island is one of the barrier islands in the Ria Formosa lagoon system, located on the southern coast of Portugal (Algarve region). The island is approximately 6–7 km long and has a curving planform oriented roughly WSW–ENE on its western side and E–W on its eastern side. It is bounded by the Faro-Olhão Inlet on the west and the Armona Inlet on the east (Figure 1). These inlets exemplify two contrasting regimes: Faro-Olhão is a fixed inlet stabilized by two long jetties (constructed 1929–1955), while Armona is a natural migrating inlet with a large ebb-tidal delta. The presence of the jetties has disrupted the natural sediment bypassing and alongshore drift at the western end of Culatra, contributing to sediment deficit and erosion. In addition, a stone revetment was constructed along the western ~1 km of the island (fronting the village of Culatra) to protect it from erosion – further limiting sediment exchange between the dune and beach in that segment. In contrast, the eastern end of Culatra has benefited from sediment accumulation associated with the Armona inlet delta. The ebb delta acts as a reservoir that feeds the adjacent shore; since the mid-20th century, Culatra's eastern tip has elongated significantly eastward and southward onto the delta platform. This natural land growth has formed new back-barrier embayments that have gradually infilled and developed into marshes in the shelter of the expanding island. The central portion of Culatra transitions between these two end-member conditions, with wide beaches and low dunes in some areas and narrower, higher dune ridges in others, reflecting a patchwork of sediment sources and sinks. The regional wave climate is dominated by Atlantic swell and sea waves from the west and southwest, which are responsible for the majority of longshore sediment transport. The western flank of the Ria Formosa barriers faces these dominant W–SW waves and tends to have a reflective beach morphotype with higher dunes and berms. The eastern flank (including Culatra's eastern end) is more sheltered from W–SW waves due to the shadowing effect of Cape Santa Maria and the rest of the island chain, and is exposed to less frequent, lower-energy waves from the E–SE. As a result, the eastern beaches are generally flatter (intermediate morphotype with finer sand) and the dunes there are lower in elevation. During very large SW storms, however, refracted wave energy can still reach the eastern sections (historical records note overwash events even on the "sheltered" side during extreme events) (Kombiadou et al., 2024). Tides in the area are semi-diurnal with a mean spring range of ~2.8 m, so water levels during storms can significantly modulate the elevation of wave runup on the beach (Garzon et al., 2022)

Net littoral drift in this region is directed eastward under the prevailing wave conditions. This means sediment eroded from Culatra's western sector or delivered to the coast by the Faro-Olhão inlet tends to be transported along the island toward the east. However, the jetties at Faro-Olhão largely block the natural eastward transport of sand from the updrift coast (Praia de

https://doi.org/10.5194/egusphere-2025-2384
Preprint. Discussion started: 26 June 2025

Faro), causing downdrift erosion. The sediment budget is therefore imbalanced: the westernmost part of Culatra (near the jetty) is sediment-starved, while the eastern part gains sediment from both the island's longshore transport and the nearby inlet/delta system. These alongshore gradients in sediment availability have produced chronic erosion of ~1–2 m/yr at the west end and sustained progradation at the east end in recent decades (apart from episodic storm setbacks) (Kombiadou et al., 2024). Topographically, the western half of Culatra features dunes up to ~6 m above mean sea level (MSL) in some sections, but dune height tapers off toward the east. In the central-eastern sector, roughly the first 1–3 km from the Armona inlet, dune elevations are as low as 2.5–3 m MSL in places (Garzon et al., 2022). Such low dunes are highly susceptible to overwash when storm surge and wave run-up exceed their crest. Indeed, historical accounts and recent observations indicate that the eastern sector has experienced overwash into the backbarrier on multiple occasions (Kombiadou et al., 2024). Previous studies in Ria Formosa have noted that island segments with lower dunes tend to be more dynamic and prone to retreat (Kombiadou et al., 2024). Conversely, sections with higher, well-vegetated dunes and ample backshore width (like parts of Culatra's west-central area) can resist storms with only minor shoreline fluctuations.

In summary, Culatra Island presents a scenario of *alongshore heterogeneity*: an eroding, human-influenced west end; an accreting, sediment-rich east end; and a middle zone that can swing between erosion and accretion depending on storm activity and sediment redistribution. This makes it a compelling site to study how models handle coupled shoreline and dune evolution under varying conditions.

https://doi.org/10.5194/egusphere-2025-2384
Preprint. Discussion started: 26 June 2025

145

Figure 1. Study area map showing the location and geomorphological setting of Culatra Island within the Ria Formosa barrier-lagoon system, southern Portugal. The western sector is sediment-starved due to anthropogenic modifications (Faro-Olhão jetties), while the eastern sector experiences accretion influenced by the Armona Inlet ebb-tidal delta. (© Google Earth)

3 Data Sources and Model Forcings

150 ### 3.1 Topographic Surveys and Remote Sensing Data

High-resolution topographic data of Culatra Island were obtained from LiDAR (Light Detection and Ranging) surveys conducted in November 2009 and November 2011. These surveys, carried out by the Portuguese Hydrographic Institute, provide digital elevation models (DEMs) of the subaerial island with horizontal resolution on the order of 1 m and vertical accuracy ~10–15 cm. The 2009 LiDAR dataset was used to initialize the model (shoreline and dune morphology pre-storm),
155 while the 2011 LiDAR served as an end-point for validation of model-predicted changes. From the DEMs, we extracted shoreline and dune positions by identifying the elevation contours corresponding to the mean sea level line (for shoreline). The dune foot and dune crest were identified from cross-shore elevation profiles using the PyBeach Python package (Beuzen,

https://doi.org/10.5194/egusphere-2025-2384
Preprint. Discussion started: 26 June 2025

2019), which applies a suite of automated algorithms, including a machine learning-based method, to detect key morphological features. Because the dune foot is not always clearly defined in raw elevation data (especially for low dunes or flat beach profiles), we also employed remote sensing for additional validation of dune positions.

Satellite-derived shorelines and dune lines were extracted using the CoastSat toolkit (Vos et al., 2019), applied to multispectral imagery from Landsat missions 5, 7, and 8. To extract shorelines, the Modified Normalized Difference Water Index (MNDWI) was computed and thresholded using Otsu's method to delineate the land–water interface. Shoreline positions were then corrected for tidal water level at the time of image acquisition by horizontally shifting the shoreline based on the difference between the instantaneous water level and mean sea level, assuming a uniform beach slope of 10% (estimated from LiDAR 2009 survey). For dune lines, the same CoastSat workflow was applied, substituting MNDWI with the Normalized Difference Vegetation Index (NDVI) to capture the seaward limit of vegetated dunes. NDVI-based thresholding enabled consistent mapping of the dune foot position across time, with the Otsu threshold adjusted within a range of 0.05 to 0.1 to optimize vegetation line detection. This semi-automated approach enabled the extraction of time series for both shorelines and dune lines from 2009 to 2011, supplementing the LiDAR surveys.

3.2 Offshore Wave Forcing Correction and Nearshore Transformation

Offshore wave data from the Faro buoy and the European Centre for Medium-Range Weather Forecasts (ECMWF) ERA5 dataset were analyzed to derive nearshore wave forcing. The Faro buoy, operated by Instituto Hidrográfico (IH), provided wave measurements from 2009 to 2011 at 36°54′17″N, 7°53′54″W, approximately 6.5 km south of Ria Formosa and within ~1 km of the ERA5 virtual grid point. This spatial proximity ensures a high degree of comparability between the two datasets. The buoy recorded significant wave height, mean wave period, and mean wave direction at three-hour intervals, except during storm events, when sampling became more frequent (approximately every 30 minutes to 1 hour). In contrast, ERA5 provides wave data at regular hourly intervals. Notably, data gaps in the Faro buoy record were observed during some storm events, which posed limitations for direct comparisons and corrections during peak conditions.

A simple linear correction was applied to both wave height and wave period. ERA5 wave heights were systematically underestimated during storm events, so we fit a linear regression between ERA5 and buoy-observed Hs and applied the resulting correction equation:

$$Hs_{corrected} = \frac{Hs_{ERA5} - 0.21}{0.69} \qquad (1)$$

This adjustment significantly improved correlation ($R^2 = 0.91$) and removed the negative bias **(Appendix A, Figure A1a)**

https://doi.org/10.5194/egusphere-2025-2384
Preprint. Discussion started: 26 June 2025

For wave period, ERA5 showed a negative bias of approximately 2 seconds. A similar regression-based correction was applied using:

$$Tp_{corrected} = \frac{Tp_{ERA5} - 0.31}{1.36} \quad (2)$$

This correction reduced the RMSE and scatter index while removing the bias **(Appendix A, Figure A1c).**

For wave direction, a uniform correction was not sufficient due to sector-dependent biases. Therefore, we applied a bias correction for each 30-degree sector, comparing ERA5 directions to buoy measurements and adjusting each sector accordingly. This reduced the average directional bias from ~20° to ~1.4°, and improved RMSE and correlation **(Appendix A, Figure A1b).**

The fully corrected ERA5 wave dataset (Hs, Tp, and direction) was used to force the SnapWave model (Roelvink et al., 2025), which transformed offshore wave conditions to hourly nearshore parameters at 26 output points spaced ~300 m apart and located ~400 m seaward of the shoreline (see calibration in Section 4.4). The unstructured SnapWave grid (Figure 2**a**), with cell sizes ranging from ~800 m offshore to ~50 m nearshore, accounted for key wave transformation processes including shoaling, depth-induced refraction, bottom friction over the ebb-delta platform, and breaking in the surf zone. These spatially variable nearshore wave conditions, illustrated in Figure 2**b**, captured bathymetric influences on local wave gradients, providing realistic inputs to the coupled shoreline and dune model in a computationally efficient manner.

https://doi.org/10.5194/egusphere-2025-2384
Preprint. Discussion started: 26 June 2025

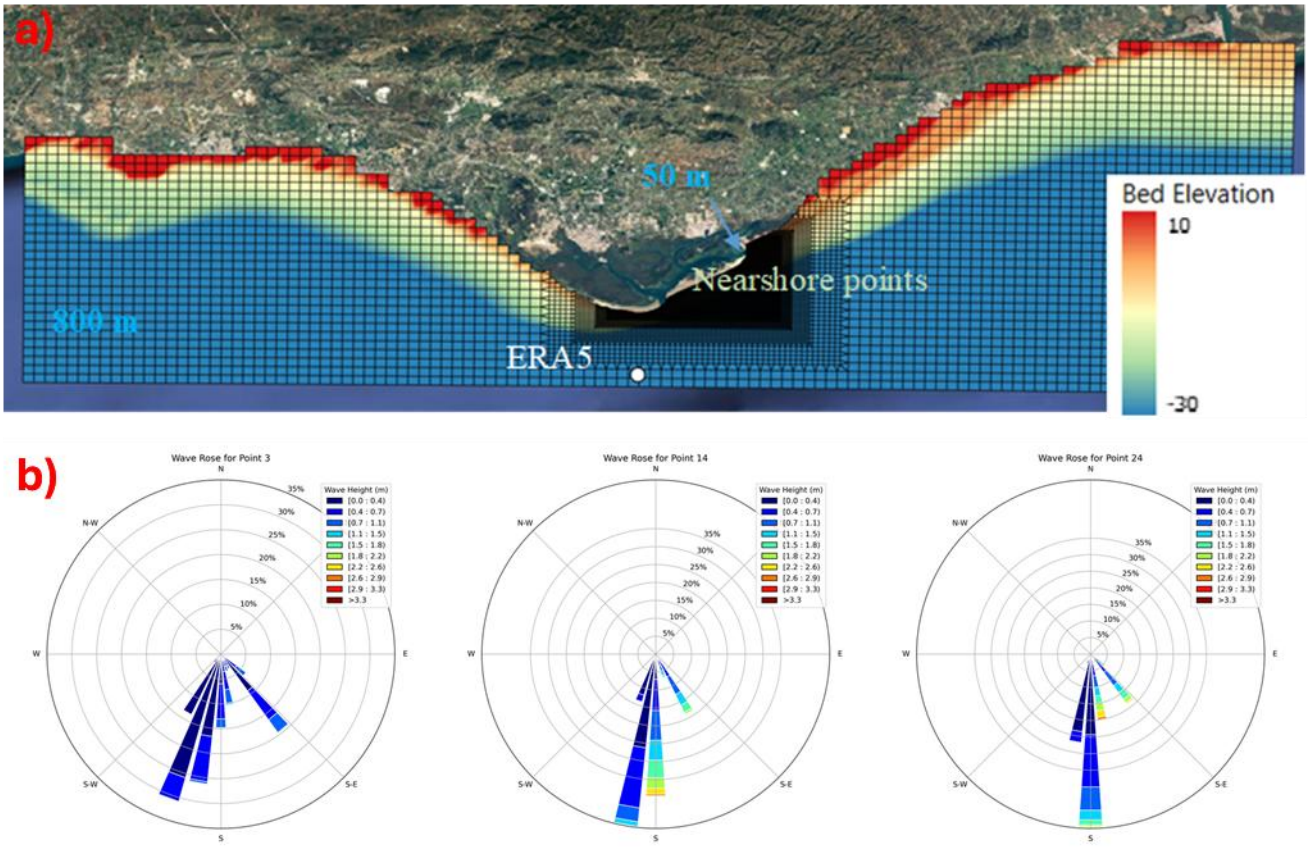

Figure 2. (a) SnapWave model domain and bathymetry used for nearshore wave transformation. Grid resolution varies from 800 m offshore to 50 m nearshore (© Google Earth) (b) Output wave points (~400 m offshore) provided spatially resolved wave conditions for input to the ShorelineS model.

3.3 Storm Event Identification

We identified thirty-one (31) storm events during the two-year study period (November 2009 to November 2011) based on offshore wave conditions corrected from ERA5 using Faro buoy data (as described in Section 3.2). A storm was defined as any period where the significant wave height (Hs) exceeded 2.5 meters for at least four consecutive hours (Figure 3**a)**. This threshold was selected to capture energetic wave conditions likely to cause morphological changes, particularly dune erosion. Using the corrected wave time series, we applied a rolling analysis to detect contiguous periods exceeding the threshold. For each storm event, we recorded the start and end times, peak Hs, peak wave period, peak wave direction, and storm duration. Overlapping or closely spaced high-energy events were merged into a single storm if the gap between them was less than 30 hours, to avoid double-counting storm clusters. This method allowed us to isolate storm durations and intensities relevant to

https://doi.org/10.5194/egusphere-2025-2384
Preprint. Discussion started: 26 June 2025

220 both alongshore sediment transport and cross-shore dune erosion processes. The 31 identified storm events (Figure 3**b**) were used to identify key drivers for morphological change in the coupled ShorelineS–dune model. Their timing is marked as vertical dashed lines in the results figures, and they served as the basis for correlation analyses between storm characteristics and modeled dune retreat in Section 5.5.

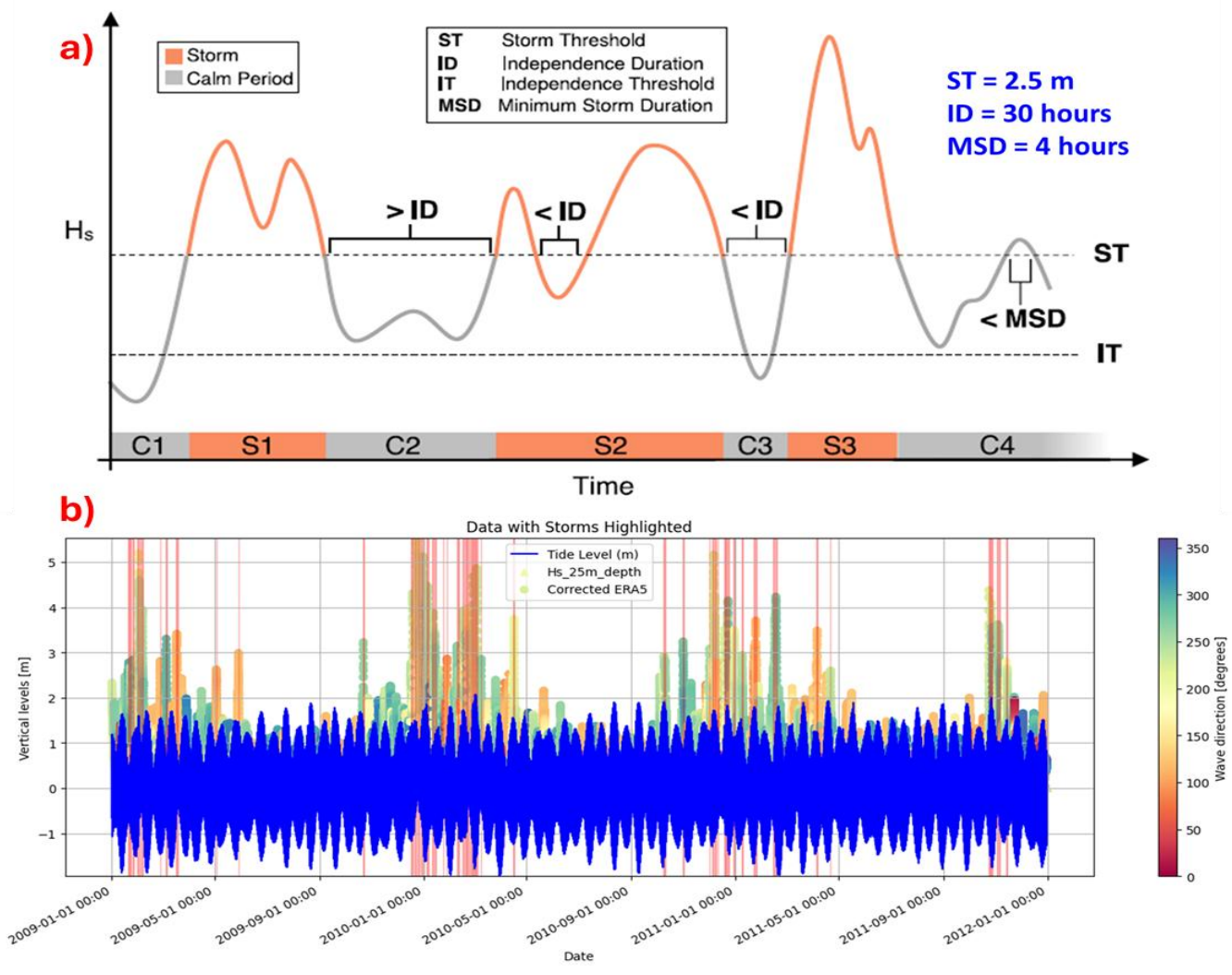

225 **Figure 3. (a) Schematic representation of storm identification criteria, including storm threshold (ST), independence duration (ID), and minimum storm duration (MSD), adapted from Kümmerer et al. (2024). (b) Time series of corrected ERA5 wave height, tide, and wave direction from Nov 2009–Nov 2011, highlighting the 31 identified storm events (red segments).**

https://doi.org/10.5194/egusphere-2025-2384
Preprint. Discussion started: 26 June 2025

4 Coupled Shoreline and Dune Model

4.1 Shoreline Model (ShorelineS)

We employed the ShorelineS model (Roelvink et al., 2020) to simulate planform shoreline changes driven by longshore sediment transport. ShorelineS is a one-line (planform) model that represents the coastline as a series of connected transects or grid points. The core of the model is the alongshore sediment transport equation, which computes changes in shoreline position *n(s,t)* based on gradients in alongshore transport ($\frac{\partial Q_s}{\partial s}$) and additional source/sink terms. In its simplest form (including sea-level rise), the governing equation can be written as:

$$\frac{\partial n}{\partial t} = \frac{1}{D_c}\frac{\partial Q_s}{\partial s} - \frac{c}{tan\,\beta}(RSLR) + \frac{1}{D_c}\sum q_i \qquad (3)$$

where D_c is the active profile height (the vertical extent of the active coastal profile from the depth of closure up to the dune crest or berm) and q_i are source/sink terms (volumetric change per unit length) due to cross-shore processes like dune erosion, overwash, nourishments, etc. This approach ensures conservation of sand volume in both the subaqueous and subaerial parts of the profile. In ShorelineS, D_c is treated as a calibration parameter that can be uniform or varied alongshore. A novel aspect of our setup was the separation of the active height into two components: one for the underwater profile (closure depth to dune foot) and one for the dune (dune foot to crest). This allowed us to specify a smaller effective active height for sections where dunes are accounted for separately, reflecting the idea that not all of the dune volume is active in alongshore transport at any given time. Conceptually, a larger D_c makes the shoreline less sensitive to a given volume change (spread over a bigger vertical extent), while a smaller D_c increases sensitivity. We used the CERC formula to compute longshore sediment transport Q_s as a function of breaking wave conditions. Specifically,

$$Q_s = bH_b^{\frac{5}{2}}sin2\varphi_i \qquad (4)$$

where H_b is the wave height, φ_i is the wave angle at breaking relative to shore-normal, and K is an empirical transport coefficient. In practice, ShorelineS offers several transport formulations; we chose the simple CERC-type relation and applied a calibration factor *qscal* to adjust its magnitude. The nearshore wave outputs from SnapWave were used to approximate breaking wave conditions at each transect (assuming local depth-limited breaking). The model time step for shoreline evolution was 1 day, aggregating the wave forcing at hourly interval for faster computation. On the other hand, the dune model time step is set an hourly interval to capture more detailed interactions especially during storm conditions.

The ShorelineS grid consisted of 85 alongshore transect points spaced 100 m apart, from the eastern tip (transect 1) to the western end (transect 85) of Culatra (Figure 4). This alongshore resolution (~100 m) is fine enough to capture significant variation in shoreline curvature and sediment gradients given the smooth nature of the island's shoreline. Each transect was assigned an initial shoreline position from the 2009 LiDAR shoreline.

https://doi.org/10.5194/egusphere-2025-2384
Preprint. Discussion started: 26 June 2025

To capture the progradation of Culatra's eastern tip onto the Armona ebb-tidal delta platform, the model domain was extended beyond the inlet-facing shoreline to include the trailing edge of the barrier. The eastern boundary was treated as a fixed-position node, allowing longshore sediment transport to accumulate at the tip but preventing outflux beyond the model domain. This approach mimics the depositional behavior observed in the growing back-barrier platform (Kombiadou et al., 2024), while conserving sediment volume within the model domain. The western boundary was landward of the Culatra jetty (no sand passes the jetty). Hard structures like the jetty can be represented by preventing transport across that point, which we ensured by our boundary setup.

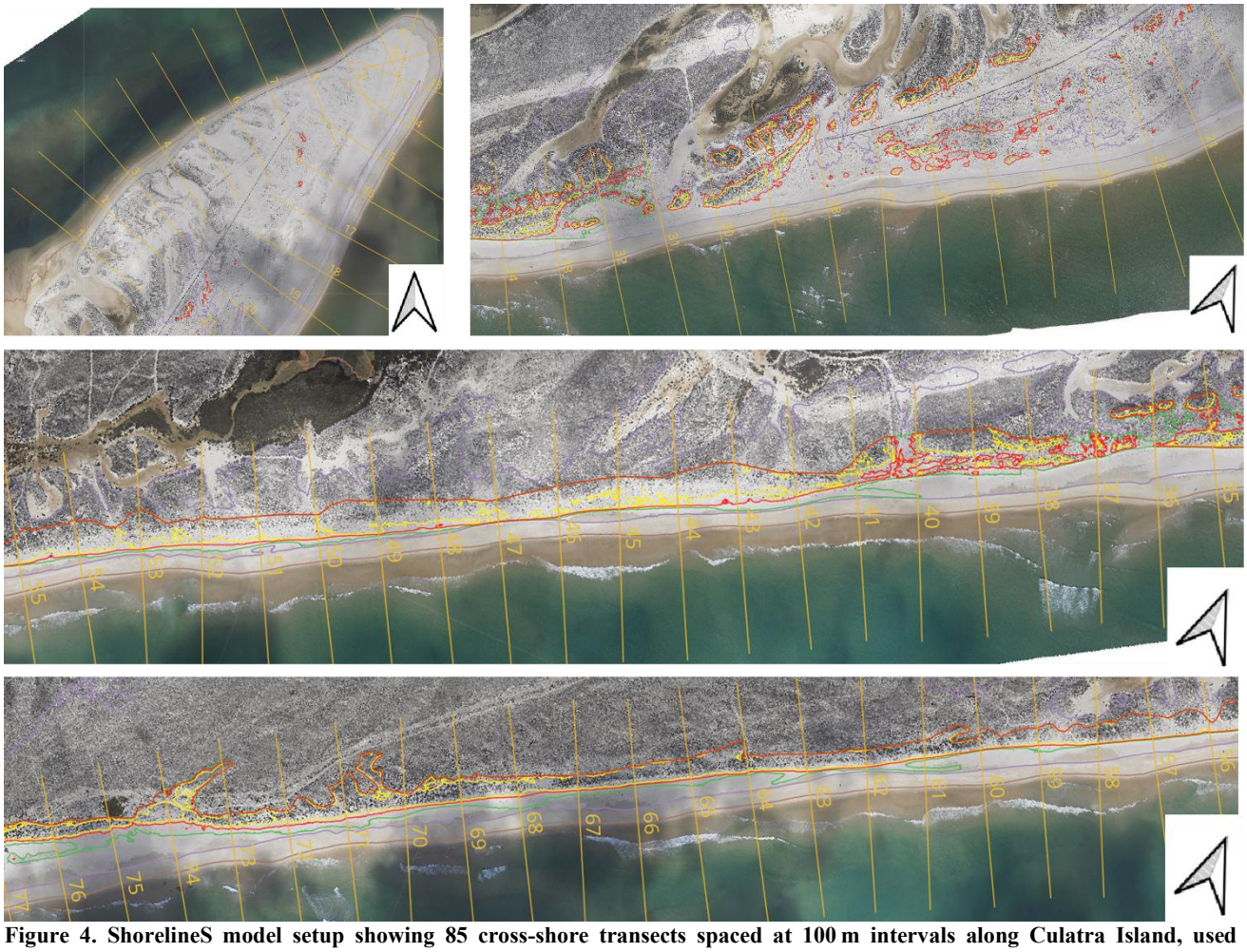

Figure 4. ShorelineS model setup showing 85 cross-shore transects spaced at 100 m intervals along Culatra Island, used for simulating alongshore shoreline and dune evolution, overlayed in 2009 orthophotos.

https://doi.org/10.5194/egusphere-2025-2384
Preprint. Discussion started: 26 June 2025

The alongshore variability described by Kombiadou et al. (2019, 2024) was also evident in the LiDAR-derived topographic profiles shown in Figure 5, which correspond to the ShorelineS transects. These profiles reveal a range of coastal responses: (i) no retreat in areas protected by seawalls, (ii) dune retreat driven by storm impacts, (iii) dune growth linked to sediment supply, and (iv) overwash processes in low-lying eastern segments. The topographic evolution captured in the LiDAR data also illustrates how PyBeach (Beuzen, 2019) effectively identifies key dune features such as the dune foot and dune crest. The automated detections align with observed erosion and overwash zones, reinforcing the utility of PyBeach for morphological analysis in storm-affected settings. These processes and their spatial variability were incorporated into our ShorelineS modeling framework, which couples shoreline evolution with storm-driven dune dynamics, as discussed in the following section.

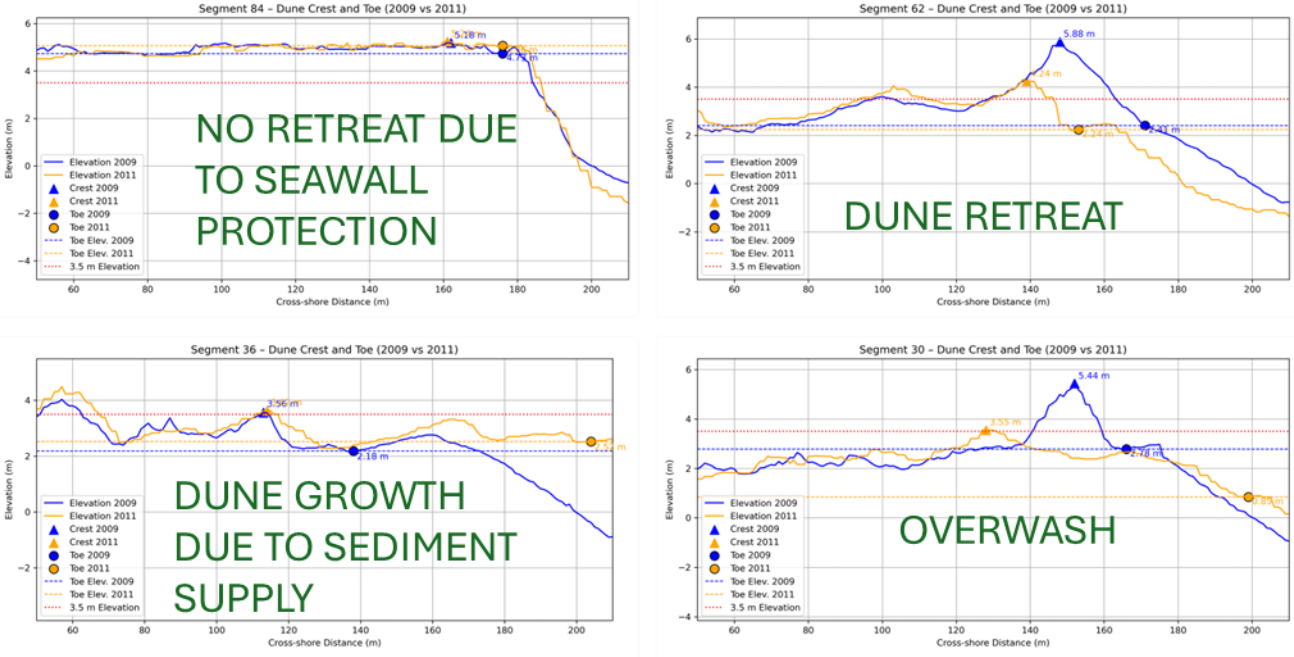

Figure 5. LiDAR-derived cross-shore topographic profiles illustrating alongshore variability in morphological response types: (i) protection by seawalls, (ii) storm-induced retreat, (iii) sediment-driven dune growth, and (iv) overwash in low-elevation zones. PyBeach detection of the dune crest and foot is overlaid.

PyBeach-derived dune morphology revealed clear alongshore variability, with lower dune crests (~2.0 m elevation) in the eastern sector and more developed, higher dunes (~3.5 m) in the central and western parts of the island (Figure 6). This elevation pattern is consistent with both the alongshore dune height variability quantified by Garzon et al. (2022) and the dune edge line manually extracted from the 2009 orthophotos, which confirms the presence of well-established, vegetated dunes in the mid and western transects. The detected dune toe and crest positions, along with the calculated berm width—defined as

https://doi.org/10.5194/egusphere-2025-2384
Preprint. Discussion started: 26 June 2025

the horizontal distance between the shoreline and the dune toe—were incorporated as inputs to the ShorelineS–dune model. In several eastern transects (Station 10 – 16), PyBeach was unable to detect a distinct dune toe and crest due to the flat topography and absence of a clear slope inflection point, highlighting known limitations of automated detection methods in low-relief terrain. In this case of missing information about a profile, ShorelineS interpolates between known adjacent profiles to initialize the coupled shore-dune model.

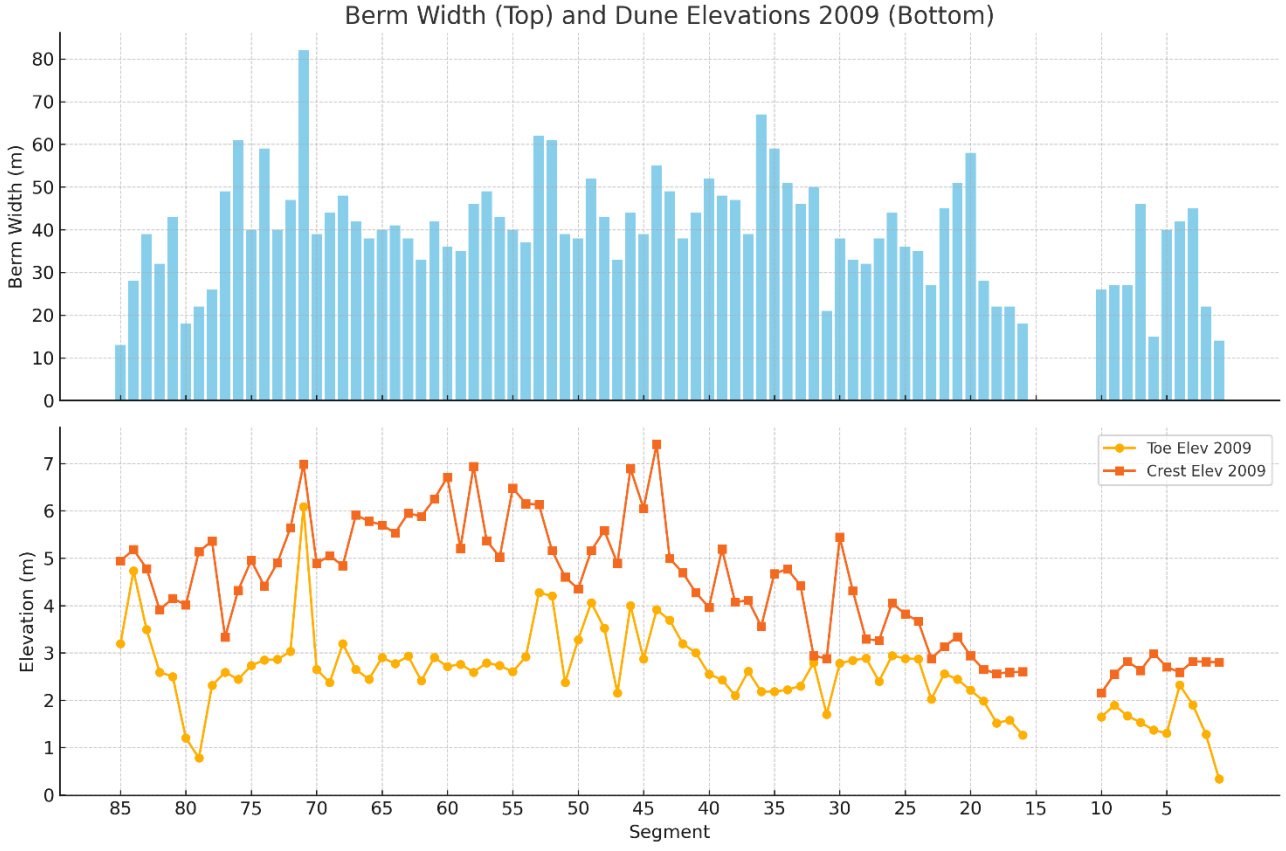

Figure 6. Input dune foot and crest elevations derived from PyBeach and corresponding berm widths (horizontal distance between shoreline and dune toe) used in the coupled ShorelineS–dune model. Stations 10–16 lacked values due to flat terrain and detection limitations.

4.2 Dune Erosion and Recovery Module

To simulate cross-shore sand exchange between the dune and beach, we integrated a dune dynamics module based on the model by Larson et al. (2016). This module accounts for two main processes: (1) Dune erosion by storm waves, and (2) Dune growth by aeolian (wind-blown) sand transport. Importantly, it provides the source/sink term q_i to the shoreline model corresponding to sand removed from or added to the beach.

https://doi.org/10.5194/egusphere-2025-2384
Preprint. Discussion started: 26 June 2025

Dune Erosion Model: We adopted the impact-based formulation where dune erosion is triggered when the total water level (wave runup R plus tide and surge) exceeds the dune foot elevation z_D. Each time step that this condition is met, a volume of sand is eroded from the seaward dune face and transported offshore. The instantaneous cross-shore sand transport rate from the dune, q_D (m³/m/s), is given by Larson et al.'s expression:

$$q_D = 4\frac{C_S(SWL+R-z_D)^2}{T} \qquad (5)$$

where C_s is an empirical impact coefficient (dimensionless) scaling the efficiency of wave impacts, and T is the characteristic swash period (taken as the deep-water wave period T_P). This quadratic formulation means that runup elevations only modestly above the dune foot cause little erosion, but much higher runup (during larger storms) greatly increases the erosion rate. No dune erosion occurs if R ≤ z_D.

We estimated the 2% exceedance runup R hourly using the Stockdon et al. (2006) formula for wave runup on beaches (based on H_S, T_P, and beach slope), adding the tidal anomaly at that time. The beach slope needed for Stockdon's formulation was estimated by the ratio of dune foot elevation and the calculated berm width.

If runup also exceeds the dune crest height, the model assumes overwash occurs. In that case, the formula for q_D is adjusted for overtopping (following Larson et al., 2009), and the eroded sand is partitioned into an offshore-directed portion q_S and an overwash portion q_L. We implemented this by specifying a dune crest height for each transect (from LiDAR, ranging 3–6 m MSL along Culatra). When R surpassed the crest, the proportion α of sand going landward was computed as:

$$\alpha = \left(\frac{R - z_D}{s}\right) - 1, for\ R > s + z_D \qquad (6)$$

where s is the dune crest height above the foot. Any overwash portion q_L was not added to the beach but assumed lost landward.

The volume of sand eroded from the dune $\frac{q_L}{\Delta t}$ (per meter length) in each time step was removed from the dune reservoir and added to the subaqueous profile seaward of the shoreline. In the one-line model context, this appears as a positive source term $q_s(x,t)$ to the shoreline equation representing a flux of sand to the beach.

Aeolian Dune Growth Model: Between storms (or on non-storm days), wind transport can gradually rebuild the dunes by moving sand from the beach to the dune. The model calculates potential aeolian transport based on wind speed, fetch distance (beach width), and grain size, following an exponential decay to an equilibrium transport rate (e.g. Lettau & Lettau, 1978; Bagnold-type formulations).

https://doi.org/10.5194/egusphere-2025-2384
Preprint. Discussion started: 26 June 2025

The model computes a potential sand transport rate q_w (in m³/m/s) and distributes it across the beach width; any sand reaching the dune foot is added to the dune (dune accretion) while depleting the beach sediment. Larson et al. (2016) calibrated the aeolian transport by specifying a threshold shear velocity for sand movement and an efficiency factor. Based on calibration, the wind friction factor was such that a 10 m/s onshore wind would transport on the order of 10^{-5} m³/m/s of sand.

4.3 Model Coupling and Integration:

The shoreline and dune components were coupled within each model time step (1 hour). At each transect and each step, the model checks the water level and wave conditions. If storm criteria are met (water level > dune foot), dune erosion is computed (removing a volume ΔV_dune from the dune). This volume is added as an instantaneous source to the shoreline model:

$$q_s = +\frac{\Delta V_{dune}}{\Delta t} \qquad (7)$$

If wind conditions are favorable for transport and waves are below the erosion threshold, the model computes dune accretion. The shoreline position and dune foot position evolve simultaneously, exchanging sand.

4.4 Model Calibration (qscal, variable active heights)

The one-line shoreline model was calibrated using a scaling factor for alongshore transport (qscal) and a variable active heights. These parameters control how responsive the shoreline is to sediment fluxes. Due to the large nearshore wave energy (Figure 2**b**), a qscal value of 0.3 was needed to calibrate the model. After this, we adjusted the active profile height (*Dc*). We employed a spatially varying active height based on depths from SnapWave output, effectively splitting the active profile into underwater and dune components. This novel approach recognizes that not all dune volume is active in longshore transport at any given time

https://doi.org/10.5194/egusphere-2025-2384
Preprint. Discussion started: 26 June 2025

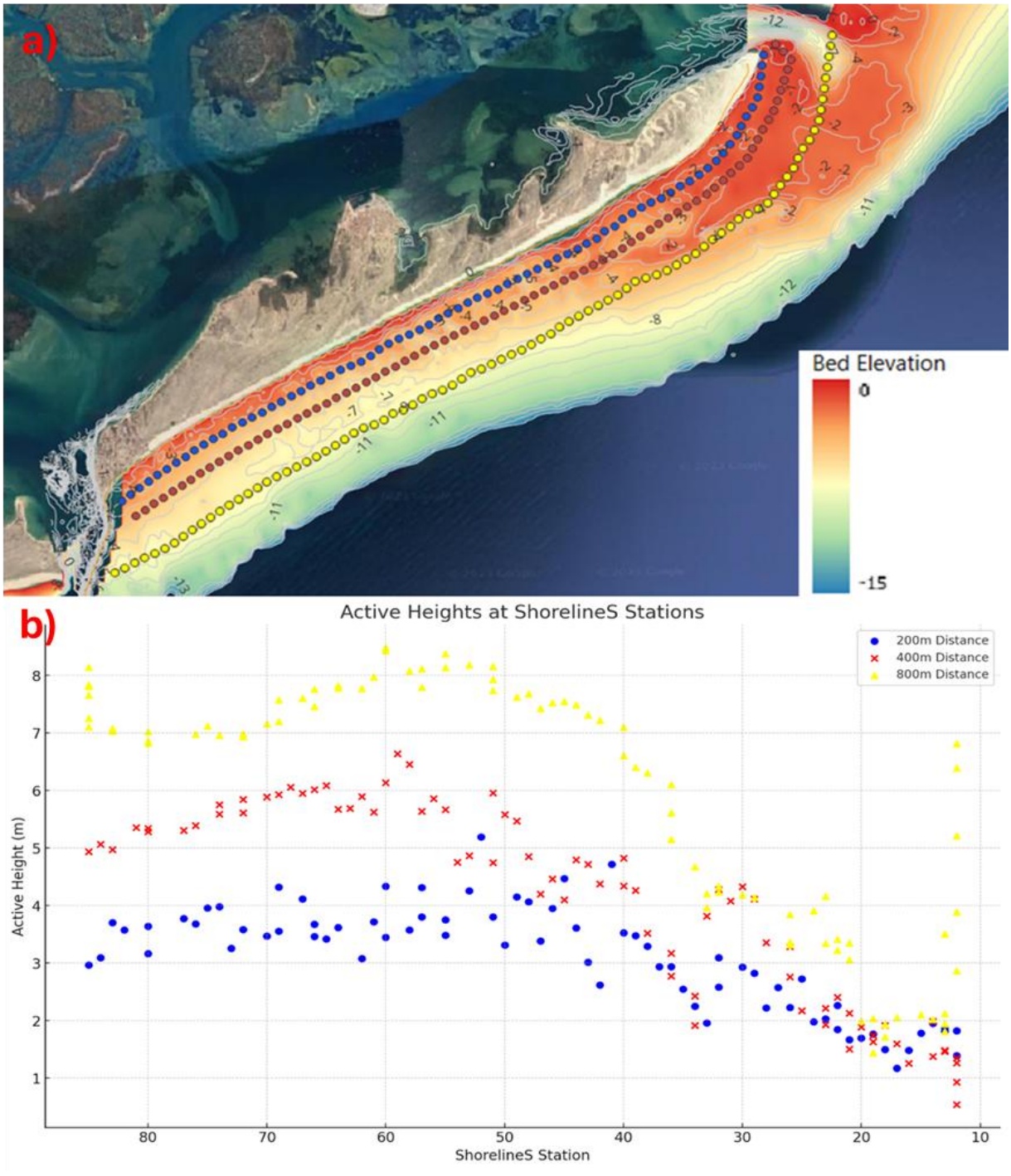

Figure 7. Model calibration using SnapWave nearshore wave output at 200, 400, and 800 m offshore distances. a) observation locations (© Google Earth) b) resulting spatial distribution of active profile heights. Eastern sector shows shallow active heights over the ebb delta.

https://doi.org/10.5194/egusphere-2025-2384
Preprint. Discussion started: 26 June 2025

Figure 8 illustrates the calibration performance of the ShorelineS model using SnapWave-derived nearshore wave data at varying distances (200 m, 400 m, and 800 m offshore). Among these, a distance of 400 m provided the best calibration with R^2 of 0.4, yielding the highest correlation with observed shoreline change. This distance struck an effective balance between nearshore resolution and stability of wave input, allowing the model to better represent local sediment transport gradients. The calibration used spatially variable active profile heights and sediment transport scaling factors (qscal), enabling the model to align with observed shoreline dynamics across different morphologic settings.

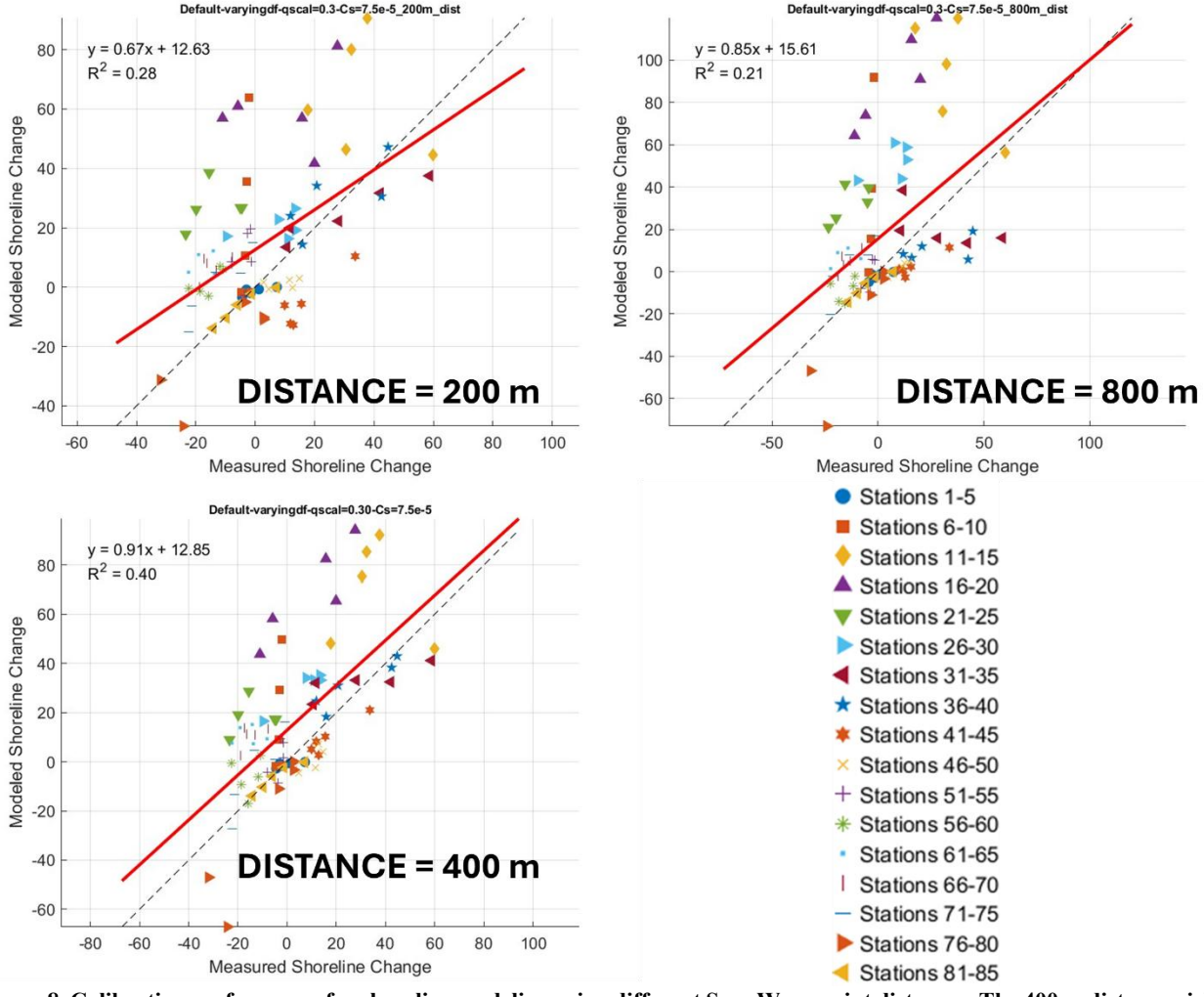

Figure 8. Calibration performance for shoreline modeling using different SnapWave point distances. The 400 m distance yielded the highest R^2 and best match with observed shoreline changes across the study domain.

https://doi.org/10.5194/egusphere-2025-2384
Preprint. Discussion started: 26 June 2025

Figure 9 compares modeled and measured shoreline change across the island from 2009 to 2011. The model produced a net shoreline change of 15.55 m and an average change of 31.70 m, compared to the measured net of 2.24 m and average of 19.35 m. The resulting bias was –12.78 m, with a root mean square error (RMSE) of 26.38 m, indicating a clear overestimation in the magnitude of change. In the western sector, modeled erosion was more severe than observed, while in the eastern sector, accretion was greatly exaggerated. This large modeled accretion in the east likely results from the combined effect of shallow active profile heights, which limit offshore transport, and the modeled overwash events.

https://doi.org/10.5194/egusphere-2025-2384
Preprint. Discussion started: 26 June 2025

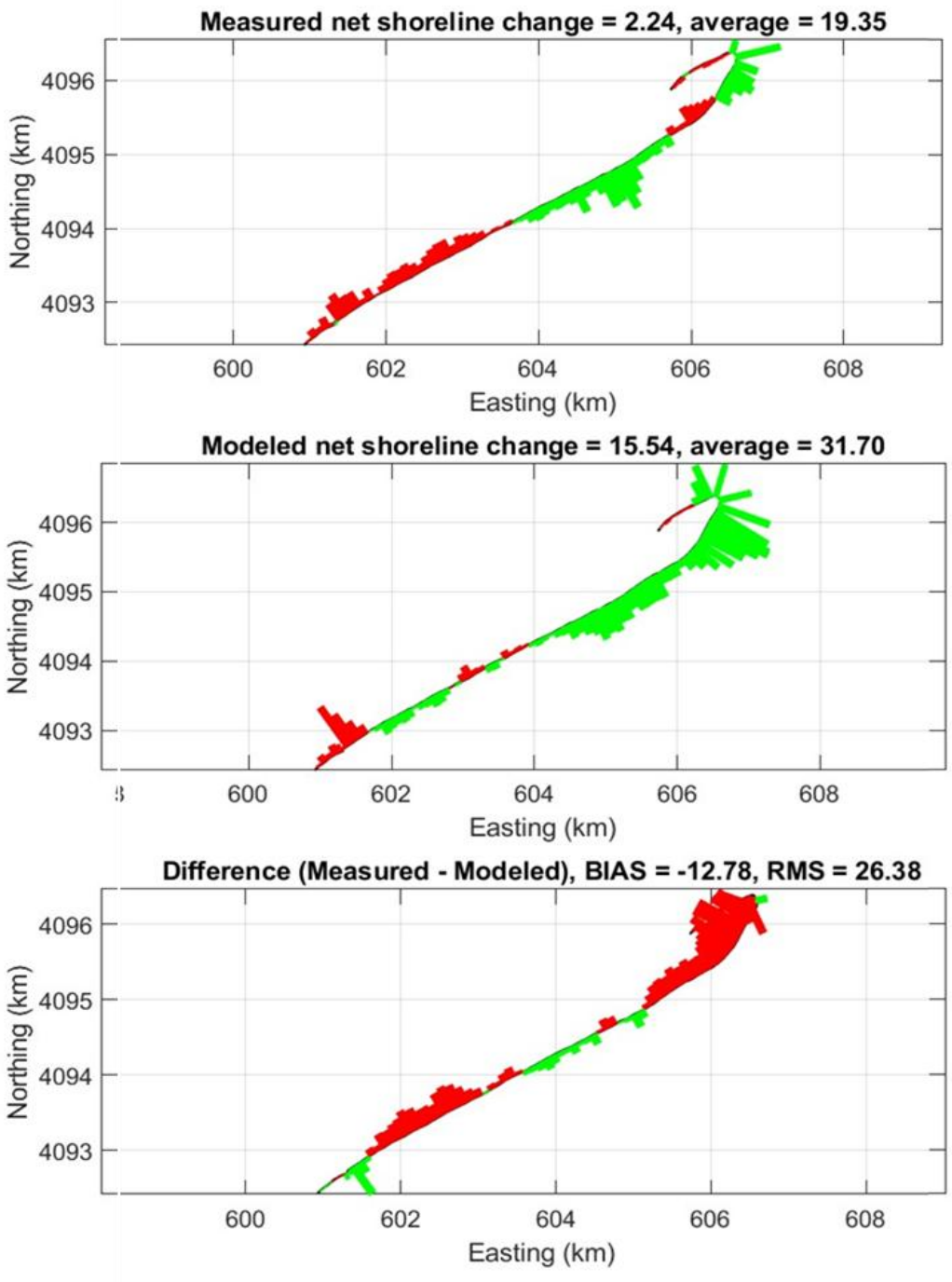

Figure 9. Modeled vs. measured shoreline change (2009–2011). Panels show: (top) observed change (net: 2.24 m), (middle) modeled change (net: 15.54 m), and (bottom) difference (bias: –12.78 m; RMSE: 26.38 m). The model overestimates accretion in the east and erosion in the west.

https://doi.org/10.5194/egusphere-2025-2384
Preprint. Discussion started: 26 June 2025

5 Results and Discussion

5.1 Model validation

After calibration, we validated the coupled shoreline–dune model against independent datasets of shoreline and dune positions. In situ lidar surveys from 2009 and 2011 provided high-resolution benchmarks for shoreline and dune foot positions at the start and end of the simulation period. However, to evaluate the model's temporal evolution and spatial variability in between those dates, we relied on satellite remote sensing. We extracted shorelines and dune vegetation lines from multispectral satellite imagery using the CoastSat toolkit (Vos et al., 2019). This approach leverages the fact that the seaward edge of dense vegetation (dune grasses) corresponds to the dune foot or foredune line. Recent studies have shown that this vegetation line is a consistent, repeatable proxy for the dune line, especially on vegetated coasts like Culatra (Garzon et al., 2022). We compiled a time series of positions (~bi-monthly frequency) for both the shoreline (wet/dry line near mean sea level) and the dune vegetation line from late 2009 to late 2011. Because satellite-derived shorelines can be biased by tidal stage at the image time, we applied a tidal correction: each extracted shoreline was adjusted vertically to mean sea level using an average beach slope of 0.1 (10%), derived from the 2009 lidar beach profiles (Figure 10**b**). This accounts for water level differences (often ±1.0 m) at image acquisition and brings the satellite shorelines to a common datum. Figure 10**a** shows the mapped dune foot/vegetation positions along the island from one such satellite mosaic, while the Figure 10**b** confirms that the tides at those image times varied by ~2 m, necessitating correction. After this processing, we obtained a set of shoreline and dune foot positions that could be directly compared to model output at corresponding dates.

https://doi.org/10.5194/egusphere-2025-2384
Preprint. Discussion started: 26 June 2025

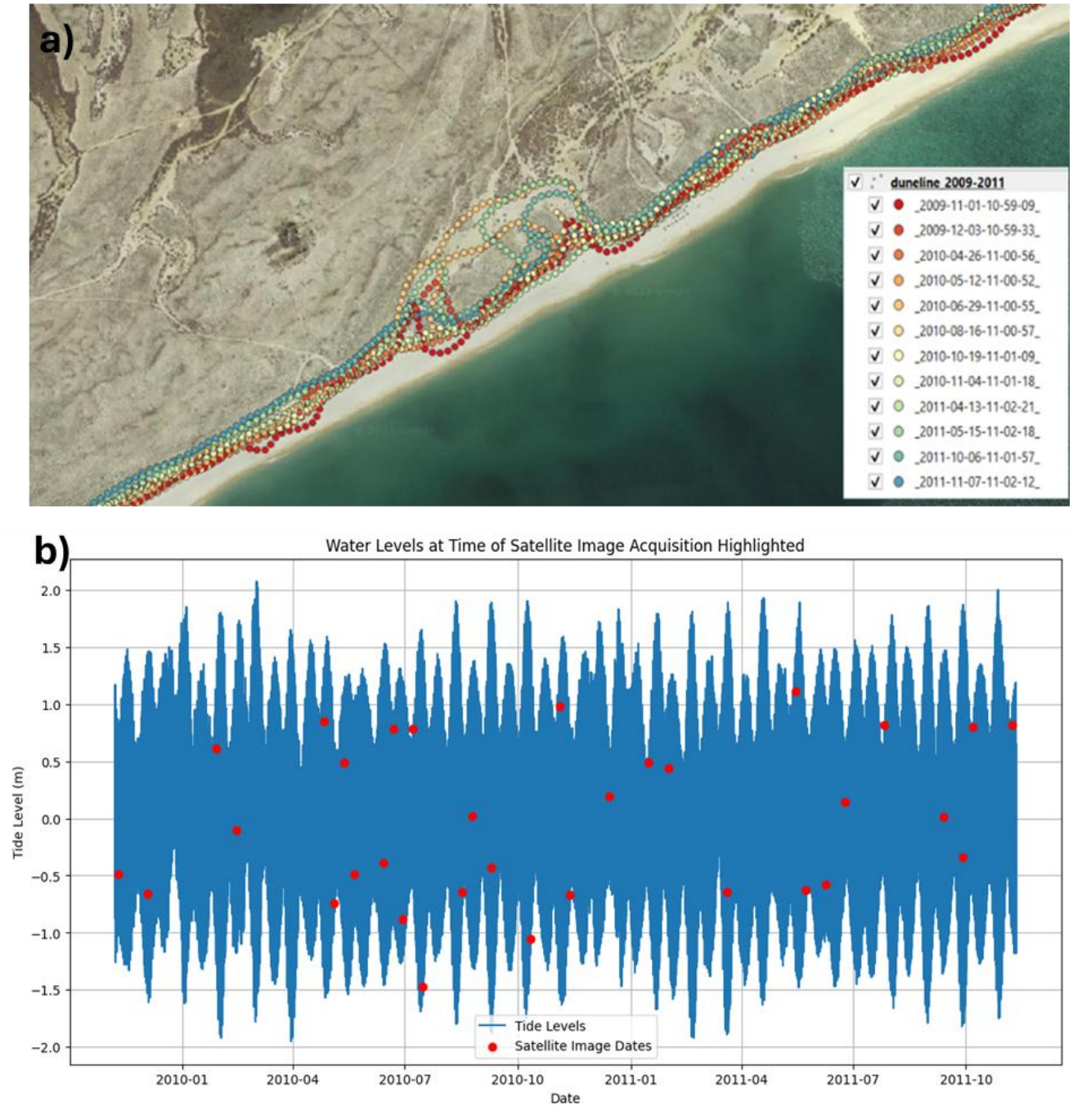

Figure 10. (a) Satellite-derived dune foot positions using CoastSat NDVI analysis (© Google Earth) (b) Tidal elevations at the time of satellite image acquisition, showing variation of ~2 m, which were used to tidally correct satellite-derived shoreline positions.

https://doi.org/10.5194/egusphere-2025-2384
Preprint. Discussion started: 26 June 2025

The model was evaluated against satellite-derived shoreline positions over time, using the coefficient of determination (R^2) to assess fit at each transect and Pearson correlation to assess trend alignment. At Station 58 (Figure 11), the shoreline model captured the general trend of retreat and the timing of storm-driven changes, though it underpredicted the magnitude of some shifts. The correlation at this location was moderate ($R^2 = 0.20$), with an RMSE of 7.40 m. The model showed consistent shoreline response to major storm events, highlighted by vertical lines, but some deviation from observed positions likely reflects limitations in storm magnitude representation and post-storm recovery or uncertainties and limitations in the satellite data.

In contrast, the dune model performs poorly, with $R^2 = -3.33$, $r = 0.24$, and an RMSE of 20.48 m, indicating large discrepancies from satellite-derived dune positions. While the model captures some long-term trend (as reflected in the modest r), it significantly over- or underpredicts the dune toe location throughout the simulation. This discrepancy likely results from the limited representation of cross-shore dune processes, such as runup-triggered erosion and post-storm recovery, as well as uncertainties in the satellite-derived dune foot detection.

https://doi.org/10.5194/egusphere-2025-2384
Preprint. Discussion started: 26 June 2025

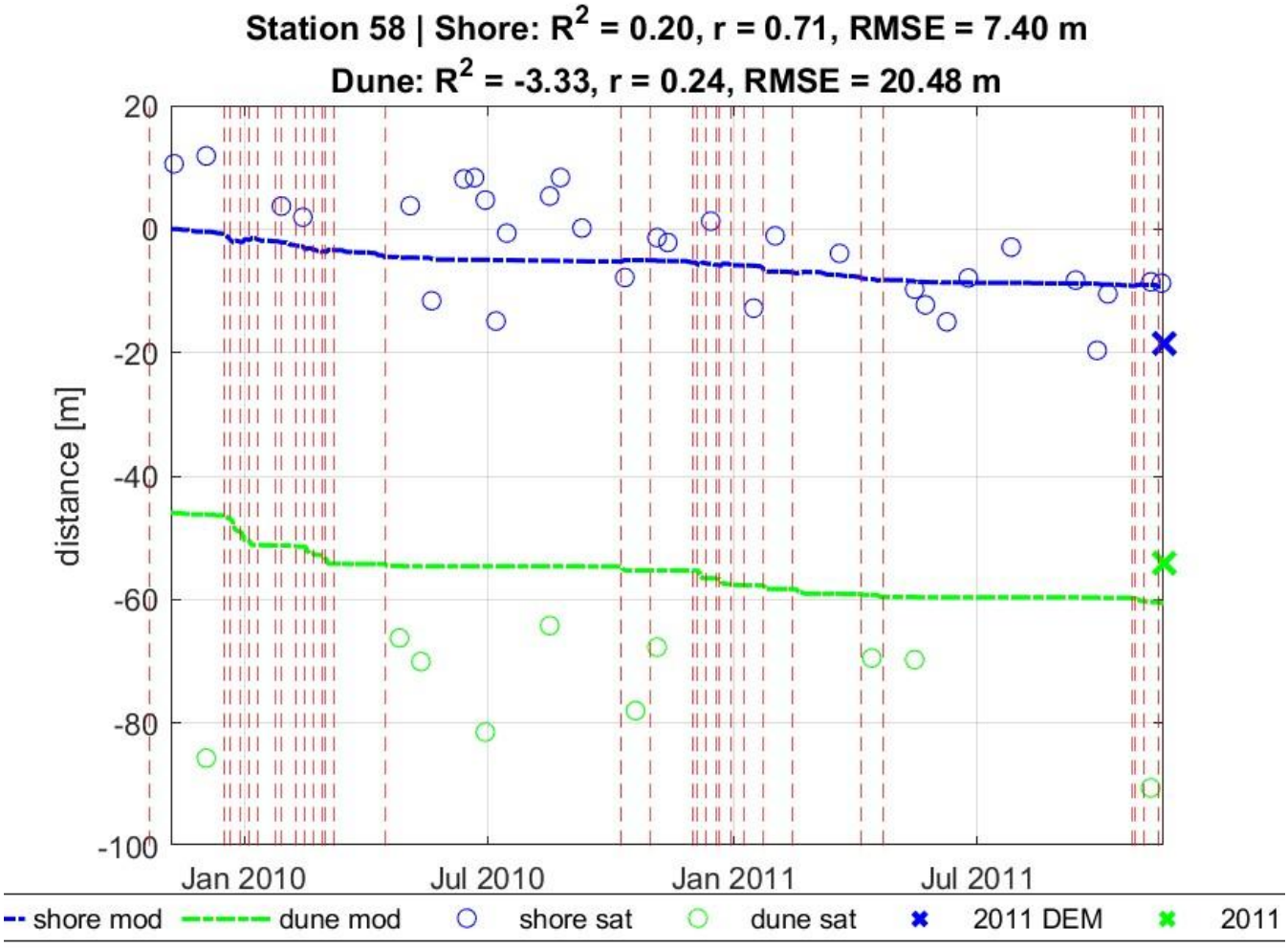

410 **Figure 11. Validation of modeled shoreline (dashed blue) and dune foot (dashed green) positions against satellite-derived (circles) and LiDAR (crosses) observations at Station 58. Vertical dashed lines denote storm events. Shoreline model shows moderate skill (R^2 = 0.20), while dune model performance is weaker (R^2 = –3.33), reflecting process and data limitations.**

Figure 12 shows the coefficient of determination (R^2) versus the Pearson correlation coefficient (r) for shoreline and dune
415 model validation across 85 stations, categorized by alongshore groups. Shoreline results are shown as open blue symbols, while dune validation results are represented by filled green symbols.

Shoreline model performance exhibits considerable variability across stations. The majority of shoreline stations display low to moderate r values (<0.6) and negative R^2, indicating that while the model sometimes captures the direction of shoreline change, it struggles to reproduce the magnitude or variability of satellite-derived observations. However, a subset of stations

https://doi.org/10.5194/egusphere-2025-2384
Preprint. Discussion started: 26 June 2025

(Stations 34 to 38) demonstrates strong performance, with both $r > 0.6$ and $R^2 > 0$, suggesting that the model accurately simulates both the trend and variance of shoreline position in those areas.

Dune validation relied on NDVI-derived vegetation lines as proxies for dune foot position, which were available only at middle and western part of the island (Station 37 to Station 85). While R^2 values for dunes were mostly negative, Figure 12 shows that most dune stations exhibited positive Pearson correlations ($r > 0$), suggesting that the model often captured the general retreat trend even if it misestimate magnitudes.

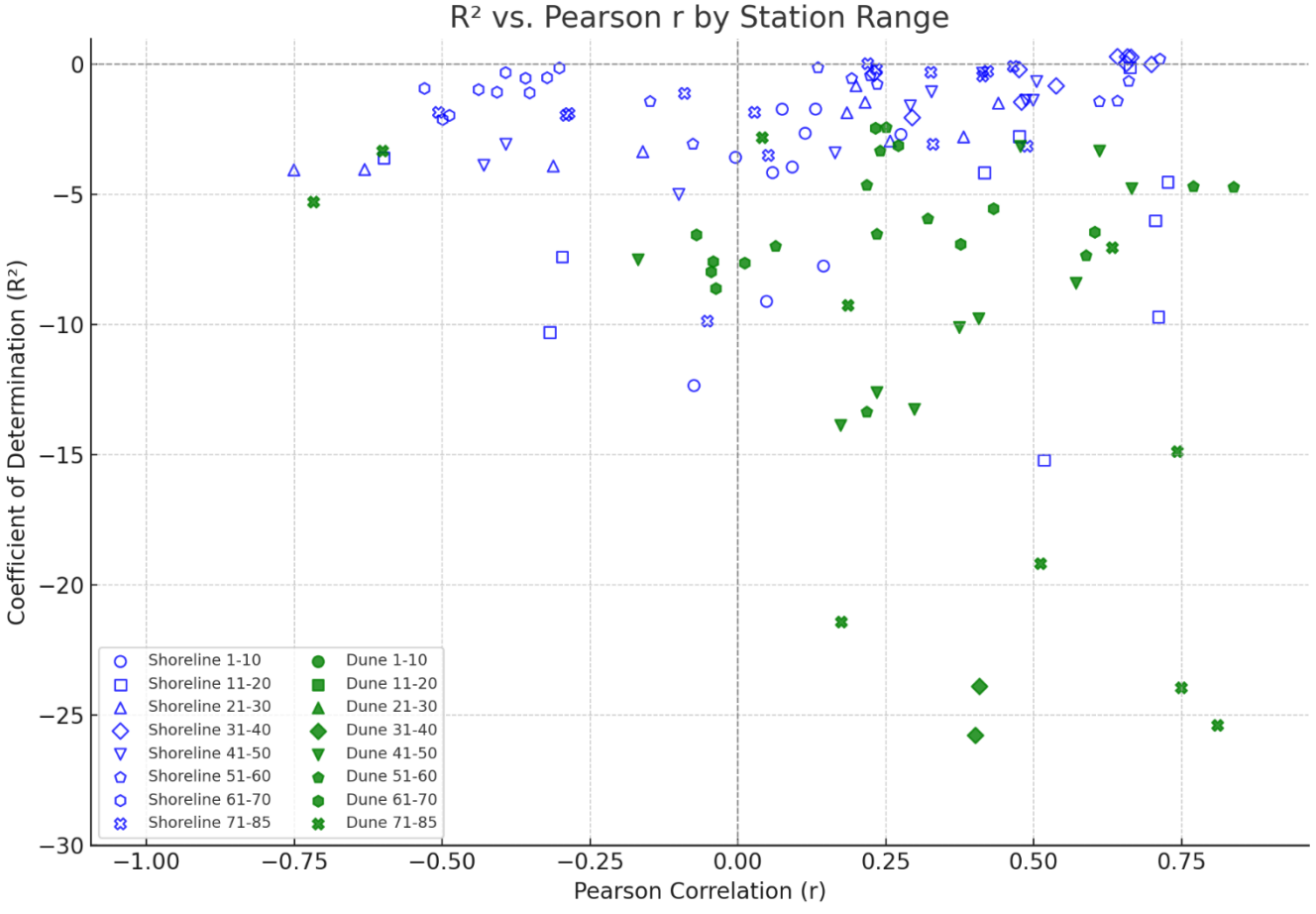

Figure 12. R^2 vs. Pearson r between modeled and satellite-derived shoreline (open blue) and dune (filled green) positions across 85 stations, grouped by alongshore segments. Most shoreline stations show low R^2 but moderate r, indicating partial trend capture but limited accuracy. Stations 34–38 show strong agreement in both metrics. Dune validation is only available at Station 37 onwards, where the model aligns with the trend ($r < 0.3$) but underperforms in magnitude ($R^2 < 0$).

While the shoreline model showed moderate agreement with satellite-derived positions, the dune model performance was weaker, with many transects showing negative R^2 values. However, this does not necessarily imply that the model poorly

https://doi.org/10.5194/egusphere-2025-2384
Preprint. Discussion started: 26 June 2025

represents dune erosion. Rather, the observed positions (NDVI-based vegetation lines) are proxies for the dune foot and may not always correspond to the exact morphological edge of the dune, particularly after storm events.

NDVI-based vegetation indices reflect the health and presence of vegetation, which can lag behind or deviate from the physical dune toe due to delayed regrowth, vegetation die-off, or partial burial. This discrepancy is supported by studies such as Zarnetske et al. (2012) and Levin & Ben-Dor (2004), which demonstrate that NDVI lines often mark ecological—not purely geomorphological—boundaries.

Additionally, Castelle et al. (2021) showed that satellite-derived shoreline positions can have errors exceeding 30 m during low tide imagery due to exposed intertidal features and tidal correction uncertainties. These issues likely apply to dune lines as well. Despite applying tidal corrections and filtering low-quality imagery, residual errors remain.

Therefore, while NDVI-derived lines enabled useful first-order spatial validation—highlighting erosional hotspots and accreting sectors—the poor correlation in time series at some transects reflects both limitations in satellite-based detection and inherent storm-driven variability in dune morphology.

5.2 Alongshore Variability of Shoreline Change and Dune Erosion Hotspots

The model results reveal pronounced alongshore variability in both shoreline and dune responses to the 2009–2011 storm sequence. Figure 13 provides a synoptic view of the island's evolution, plotting shoreline (top panel) and dune foot (bottom panel) position changes over time along the 7 km stretch. Several key patterns emerge. First, long-term erosion in the west and accretion in the east are clearly reproduced: transects near the western jetty (approximately T71–T85) show consistent shoreline retreat (red colors), whereas the eastern end (T1–T40) shows steady seaward advance (green colors). This gradient reflects the persistent west-to-east net littoral drift and sediment bypassing at the downdrift Armona inlet, as noted in previous studies of Ria Formosa (Garzon et al, 2022; Kombiadou et al., 2019, 2024). It should be note that T80-85 is protected by revetment so any modelled changes there is a model artifact. Notably, our model domain included the growing back-barrier platform on the eastern tip, and the simulation indeed accumulates sand there, mimicking the observed progradation of Culatra's eastern spit (Culatra is elongating eastward).

Superimposed on this regional gradient, the model captures a localized erosion "hotspot" in the central-western sector (roughly transects T42–T77) for the dunes (Figure 13**b**). In this zone, the dune foot retreats dramatically during major storms, more so than elsewhere, while the adjacent shoreline shows an interesting behavior: immediately following big storms, the shoreline at the hotspot either holds position or even advances seaward (visible as intermittent green/red streaks in the Figure 13**a** in the T50–70 range, corresponding to storm times marked by magenta vertical dashed lines). This counterintuitive shoreline advance

https://doi.org/10.5194/egusphere-2025-2384
Preprint. Discussion started: 26 June 2025

amidst a generally erosional regime is explained by cross-shore sediment exchange. In essence, the dune in the hotspot is acting as a sacrificial source of sand – storm waves erode the dune and transfer that sand to the nearshore, which bolsters the beach width and shoreline position.

This process was observed in the post-storm lidar data (Figure 5): the central part of Culatra had fresh washover fans and a flatter foreshore, indicating sand redistribution from dunes to beach. The model reproduces this by design: whenever dune erosion (positive q_s) is triggered, that volume is added to the shoreline as a source term. Our results thus support the conceptual model of dunes as a sand reservoir buffering the shoreline (sensu Sallenger, 2000's "collision regime") – intense dune collision can yield a short-term shoreline accretion or stability even under large waves, because the eroded dune sand temporarily nourishes the beach. Moreover, intense dune erosion and overwash in the east (transects 20-30) is attributed to the low dune morphology where overwash was observed in the LIDAR profiles (Figure 5) and documented in Kombiadou et al., 2024.

https://doi.org/10.5194/egusphere-2025-2384
Preprint. Discussion started: 26 June 2025

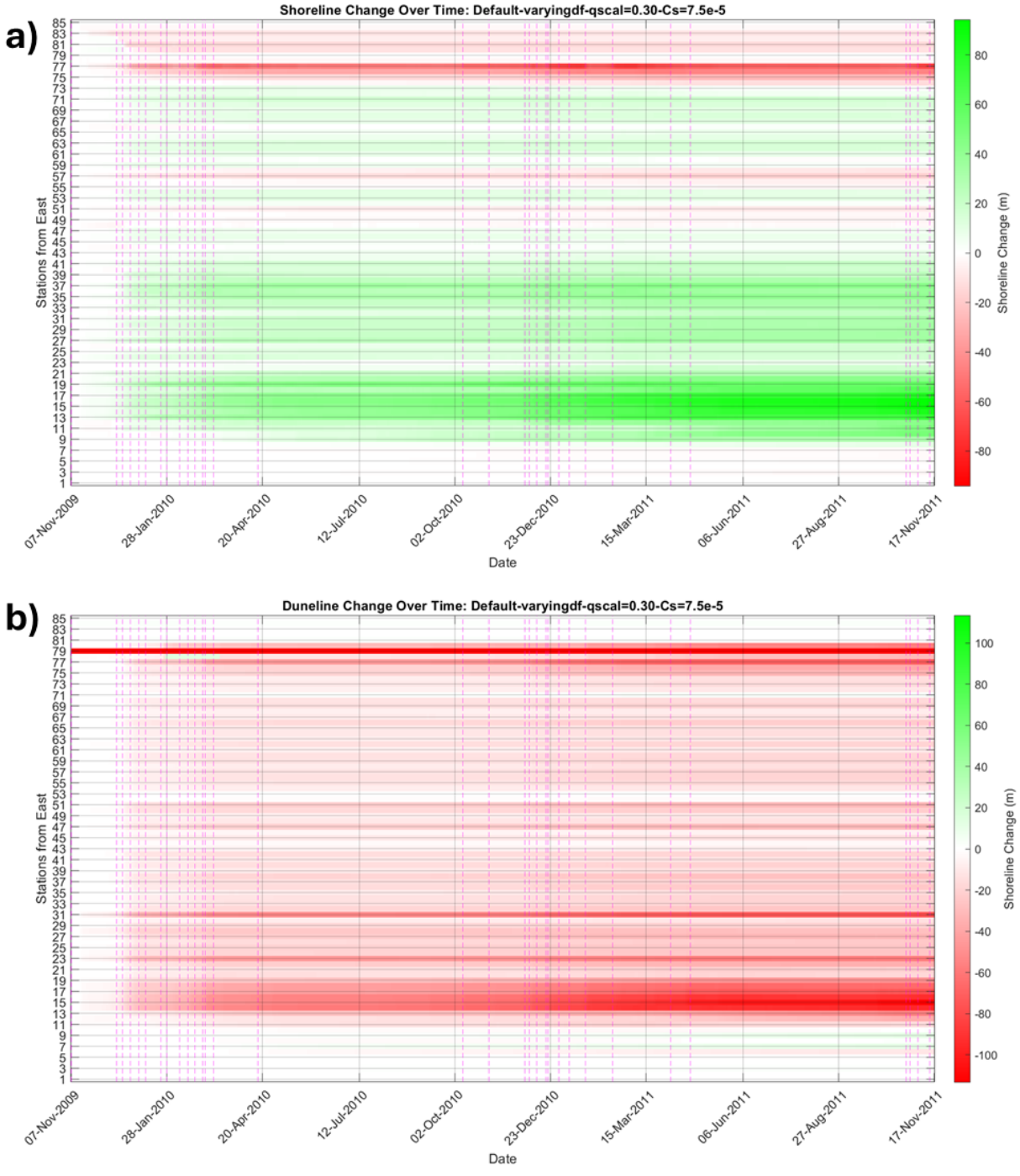

475 **Figure 13. Spatiotemporal evolution of (a) shoreline and (b) dune foot positions from Nov 2009–Nov 2011. Color gradients show erosion (red) to accretion (green). Vertical dashed lines mark storm events. A localized dune erosion hotspot is evident in the central-western sector (T42–T77), resulting in concurrent shoreline advance due to sand exchange. Intense dune erosion and overwash are also observed in the east (T20-30)**

https://doi.org/10.5194/egusphere-2025-2384
Preprint. Discussion started: 26 June 2025

5.3 Contributions of Alongshore vs. Cross-Shore Processes

To disentangle the contributions of processes, we analyzed the sediment budget terms output by the model. Figure 14 breaks down the cumulative shoreline change at each transect into components: (i) change due to alongshore transport gradients (*dSds*), essentially the one-line model's baseline result), (ii) change due to dune erosion/accretion (q_s, the source/sink from dunes), (iii) change due to overwash (q_l), which is observed at the low dune morphology in the eastern part (transect 10-20)), and (iv) change due to wind/aeolian transport (qw). Positive values indicate a contribution toward shoreline advance (accretion), while negative values indicate causing retreat.

The strongest sediment losses occurred at stations 75–80, where dSds reached down to -3.8×10^5 m²/s, coinciding with intense divergence near the groyne-influenced western inlet. Conversely, positive dSds values peaked near stations 5–10 at ~2.5×10^5 m²/s, consistent with net sediment convergence and accumulation at the downdrift eastern sector. Dune contributions (q_s) are particularly significant between stations 45–70, where values up to 0.7×10^5 m²/s indicate that eroded dune sand helped offset negative dSds and stabilize the shoreline during storms. Overwash contributions (q_l) are visible across stations 10–30, reflecting crest exceedance and landward sediment transport in areas with low dune elevations, consistent with LiDAR-based profiles of overwash-prone sectors. Aeolian transport (q_w) remains minimal, with only sparse, weak cyan bars appearing mainly in the central part of the island—indicating limited wind-driven recovery under coarse sand and short inter-storm intervals. Collectively, these patterns confirm that shoreline accretion in the eastern sector is driven by positive dSds, magnified by shallow active profile heights and supported by minor q_s and q_l contributions. In contrast, the central-western "hotspot" (stations 45–70) exhibits a compensatory relationship between negative dSds and positive q_s, revealing the importance of dune-beach coupling in modulating shoreline change. The westernmost transects (75–85) show intense retreat driven by highly negative dSds and limited compensatory fluxes—likely exacerbated by sediment entrapment upstream and the presence of a revetment.

https://doi.org/10.5194/egusphere-2025-2384
Preprint. Discussion started: 26 June 2025

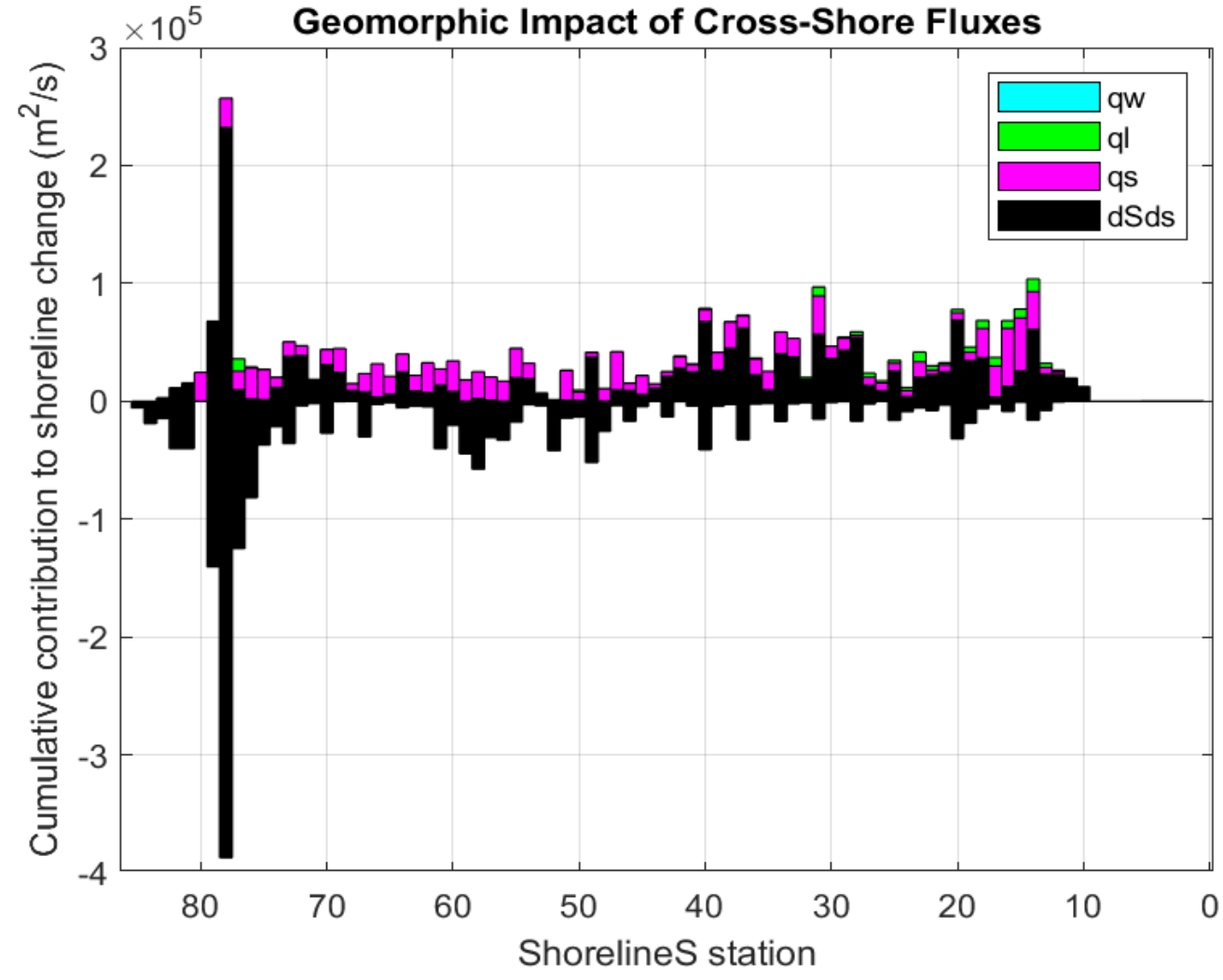

Figure 14. Cumulative contribution of individual sediment transport components to shoreline change: alongshore gradients (dSds), dune erosion/accretion (qs), overwash (ql), and aeolian transport (qw). Positive bars indicate accretionary effects; negative indicate erosional contributions. Dune–beach coupling is strongest in the central-western hotspot while overwash is modeled in the east.

From a coastal management perspective, this means that relying on alongshore sediment management alone (e.g., groins, bypassing) might underestimate the stability of certain sections if dune contributions aren't considered. It also means that if the dune in that hotspot were artificially stabilized, the beach might actually experience worse erosion there, since it would no longer receive the dune sand. This interplay is a key finding of our study: alongshore sediment transport sets the baseline trend, but cross-shore exchanges (dune erosion or overwash) can create hotspots of erosion or accretion that deviate from the trend.

https://doi.org/10.5194/egusphere-2025-2384
Preprint. Discussion started: 26 June 2025

Similar conclusions were drawn by Garzon et al. (2022), who found that spatial variations in backshore (dune+beach) morphology led to differential storm impacts and the development of retreat hotspots. In our case, the "local salient" was a higher, vegetated dune ridge in the central island which, once eroded, straightened that section of coast and yielded a hotspot.

5.4 Event-Scale Dynamics

To better understand the morphodynamic response at the event scale, we analyzed the outputs of the coupled model during a representative storm: Storm 1 (16–19 December 2009). Figure 15 presents the model-derived spatial and temporal parameters during this event. The upper panels illustrate alongshore variations in key morphological indicators, including duneline change, initial berm width before the storm, shoreline change, cumulative cross-shore fluxes (qs, ql, qw, and dSds), and maximum total water level (TWL), all resolved per station. These outputs characterize how each location along the island responded to the storm, with the most pronounced dune retreat occurring in the central region (Stations 50–70) where berm widths were narrow and total water levels elevated.

The bottom panel of Figure 15 shows the temporal evolution of offshore significant wave height (SWH) from both ERA5 and SnapWave colored by wave direction. The SnapWave-derived wave heights are consistently lower than ERA5, reflecting nearshore wave dissipation processes captured by the transformation model. These outputs provide essential storm forcing characteristics for each model segment, such as wave height time series, directional shifts, and the cumulative energy metrics used in subsequent correlation analyses.

Together, these panels summarize the primary model-derived parameters extracted for evaluating storm-scale impacts across the barrier island.

https://doi.org/10.5194/egusphere-2025-2384
Preprint. Discussion started: 26 June 2025

Figure 15. Event-scale morphodynamic response during Storm 1 (Dec 16–19, 2009). Top panels: alongshore variation in dune retreat, shoreline change, berm width, sediment fluxes (qs, qw, dSds), and total water level. Bottom panel: SnapWave and ERA5 wave height time series colored by direction, highlighting storm forcing and model response.

https://doi.org/10.5194/egusphere-2025-2384
Preprint. Discussion started: 26 June 2025

5.5 Controls on Dune Retreat: Correlations with Storm Forcing Parameters

Given the model's ability to simulate dune erosion across many storms and transects, we can statistically examine which storm factors correlate most with the modeled dune retreat. We performed a correlation analysis between the dune foot position change (retreat magnitude) and several storm parameters: cumulative cross-shore sediment flux from the dune (q_s sum), storm duration, root-mean-square significant wave height during the storm, peak wave direction, initial berm width, and peak total water level (runup + storm tide). Figure 16, presents scatter plots of these relationships for all storms and transects. The results are clear: storm duration ($R \approx 0.48$) and cumulative dune-eroded volume ($R \approx 0.73$) are the strongest predictors of dune retreat, whereas wave direction ($R \approx 0.04$) and initial berm width ($R \approx 0.02$) show little to no correlation. In other words, where and when the model produces large dune retreats correspond to long-lasting storms that remove large volumes of sand from the dune. This makes physical sense – a longer storm (or sequence of storms) provides more time for waves to eat away at the dune foot, especially once the dune is exposed and actively eroding. Wave height does correlate (higher waves tend to cause more erosion) but not as tightly as duration or energy flux, likely because even a very high wave event will cause limited erosion if it's short-lived or mostly during low tide. Our findings are consistent with field studies emphasizing total storm energy and pre-storm morphology over instantaneous metrics. For example, Masselink et al. (2016b) observed in a series of UK storms that the overall impact on dunes depended on the integrated wave energy hitting the coast over the season, and that storm groups caused more damage than isolated events. In the model, the "cumulative q_s" is essentially a proxy for total wave impact energy above the dune foot (since q_s is proportional to runup exceedance, integrated over time). The near-perfect correlation between q_s and retreat is somewhat tautological (the model is built such that they are directly linked), but it verifies internal consistency. More enlightening is that storm duration came out important – indicating that given two storms of similar energy, the longer one will cause more dune retreat, perhaps because sustained wave attack allows the beach/dune to reach a more eroded equilibrium.

On the other hand, the very weak correlation with peak wave direction confirms that, in our case, the angle of wave incidence had minimal influence on dune erosion magnitude. Most storms approached from west to southwest (the dominant direction), with some variability, but apparently whether a storm's waves were, say, 10° vs 30° oblique didn't change how much dune was eroded – as long as the waves hit the dune, they caused erosion. This aligns with the notion that once waves are large enough to collide with the dune, what matters is how many and how long, not from exactly which oblique angle. Empirical evidence supports this: Masselink et al. (2016a) reported that dunes exposed to normal-incidence waves (direct onshore attack) were heavily eroded, whereas sites with highly oblique waves saw less dune erosion even if longshore drift was intense. In our model, longshore currents (represented by alongshore transport) certainly redistribute sand but do not directly cut into dunes – that requires direct wave impact (runup exceedance). Burvingt et al. (2016) analyzed beach response to the 2013/14 UK storms using LiDAR and found that cross-shore sediment loss dominated exposed beaches, while longshore transport (beach

https://doi.org/10.5194/egusphere-2025-2384
Preprint. Discussion started: 26 June 2025

rotation) was more prevalent on oblique-facing coasts. This supports our finding that wave impact rather than angle-controlled longshore processes dominates dune erosion.

Interestingly, the minimal influence of initial berm width suggests that the spatial distance between the shoreline and dune toe did not play a significant role in determining the amount of dune erosion. While berm width might be expected to buffer the dune by absorbing wave energy or delaying the onset of impact, our results show that, once the total water level exceeds the dune foot elevation, erosion proceeds largely independent of that initial buffer. In the model, berm width influences beach slope (and thus runup) but does not directly control whether erosion occurs. This behavior reflects the dominance of the collision regime: once initiated, sustained runup exceedance is what governs erosion, not how wide the beach was prior to impact. Wider berms may delay the onset of erosion slightly, but they do not reduce the total volume removed once the dune is exposed. Similar findings were reported by Itzkin et al. (2021), who showed that while narrower beaches increase vulnerability, the magnitude of erosion is ultimately governed by storm duration and surge conditions.

We also examined the effect of peak water levels (tide + surge + runup), which in principle determine how high up the profile waves can attack. Interestingly, the model results showed only a weak correlation between maximum runup level and dune retreat extent. This could be because for all the significant storms, runup did exceed the dune foot (hence erosion occurred), and differences of, say, 0.5 m in runup height (whether runup just barely overtopped the foot vs. overtopped by 0.5 m) might not translate to markedly different erosion volumes in the model's formulation. Essentially, once the dune collision regime is triggered, the erosion rate is more controlled by how long it continues rather than how far above the threshold the runup reaches (especially since overwash was rare). Only if runup reached the dune crest to cause overwash would we expect a different mode of response (and our model would then partition sand differently). Since overtopping was uncommon, all storms mostly caused "collision" type erosion (sensu Sallenger, 2000), and within that regime the duration and wave energy flux were the dominant factors.

https://doi.org/10.5194/egusphere-2025-2384
Preprint. Discussion started: 26 June 2025

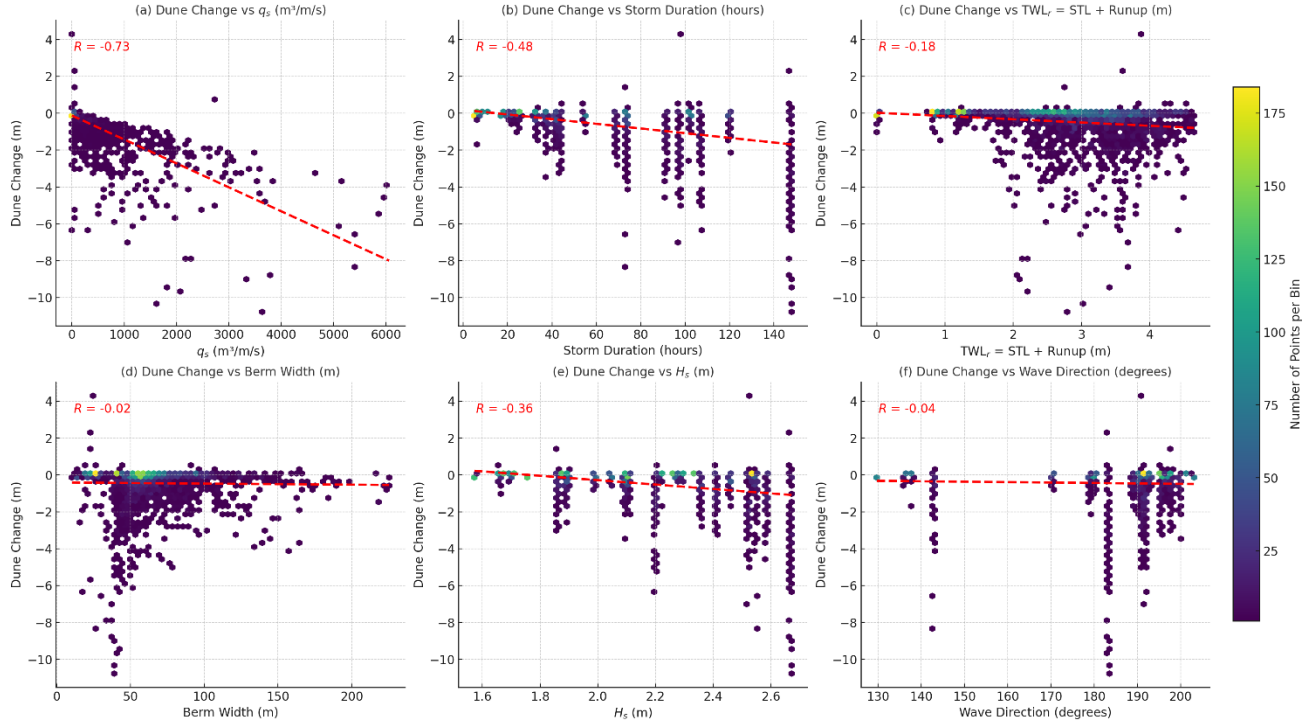

Figure 16. Correlations between modeled dune retreat and storm forcing parameters across all transects and storms. Strongest predictors are cumulative dune sand loss (qs; R = 0.73) and storm duration (R = 0.48). Peak wave direction and initial berm width show weak correlations, indicating dominance of cross-shore over angle-dependent processes.

6 Conclusions

Alongshore transport dominates regional trends, but cross-shore processes create local departures

The coupled ShorelineS–dune model successfully replicated the spatial pattern of shoreline erosion in western Culatra and accretion in the eastern sector, consistent with gradients in longshore sediment transport. These gradients were effectively modulated through spatially variable active profile heights and transport scaling factors, allowing the model to reproduce the sediment-starved west and the depositional behavior of the ebb-tidal delta in the east. Although the model overestimated the magnitude of shoreline change—particularly accretion in the east—this reflects the influence of shallow active heights and overwash-driven sand delivery.

https://doi.org/10.5194/egusphere-2025-2384
Preprint. Discussion started: 26 June 2025

Emergence of a dune erosion hotspot through dune-beach coupling

The model revealed a storm-induced erosion hotspot in the central-western sector (transects T42–T77), where intense dune retreat supplied sand to the adjacent beach, driving localized shoreline advance during storms. This highlights the importance of explicitly including cross-shore sediment exchanges in shoreline evolution models. In the eastern sector (T10–T30), modeled overwash occurred during major storm events and contributed to landward sediment redistribution, reinforcing observed shoreline progradation. These dynamics underscore that dune erosion and overwash can temporarily buffer shoreline retreat by nourishing the active beach profile. For coastal management, this suggests that maintaining natural dune dynamics—rather than widespread hard stabilization—can enhance resilience in non-critical dune areas.

Model sensitivity and calibration insights

The model demonstrated high sensitivity to the wave impact coefficient (C_s) and grain size (d_{50}), both of which were key calibration parameters for dune erosion and recovery. A calibrated $C_s \approx 7.5\times10^{-5}$—lower than the default from Larson et al. (2016)—was required to match observed retreat volumes in the erosion hotspot. This suggests that local morphodynamic conditions, such as reflective beach slopes and pre-existing dune scarps, increased the efficiency of wave impact. Additionally, the use of coarse sand ($d_{50} \approx 0.5$ mm) and low wind speeds significantly reduced modeled aeolian transport and post-storm dune recovery. These findings emphasize the need for site-specific calibration, especially in impact-based dune erosion frameworks.

Validation confirms model skill and the value of satellite-derived vegetation lines

Validation using LiDAR and satellite-derived shoreline and dune positions showed that the model reasonably captured overall shoreline evolution and storm-driven changes, though accuracy varied across stations. Shoreline model performance was moderate, with an example RMSE of 26.38 m and $R^2 = 0.20$ at Station 58, and most stations showing low to moderate Pearson correlation ($r < 0.6$) and negative R^2, indicating trend alignment but difficulty reproducing the full variability. Dune model performance was weaker, with many stations showing negative R^2; however, most dune stations still exhibited positive Pearson correlation, suggesting the model effectively captured general retreat trends despite mismatches in magnitude. This discrepancy reflects both model limitations and uncertainties in NDVI-derived vegetation lines, which act as proxies for the dune foot but may lag behind morphological changes due to vegetation die-off, delayed regrowth, or low-relief terrain. These issues are consistent with previous studies (e.g., Zarnetske et al., 2012; Levin & Ben-Dor, 2004; Castelle et al., 2021) and highlight the challenge of validating morphodynamic models using ecological proxies. Nonetheless, the NDVI dataset

https://doi.org/10.5194/egusphere-2025-2384
Preprint. Discussion started: 26 June 2025

provided spatially and temporally rich information that enabled meaningful evaluation of alongshore variability and identification of erosion hotspots.

Cross-shore storm processes—not wave angle or berm width—control dune retreat

Correlation analysis across all transects and storm events showed that cumulative cross-shore sediment flux from the dune ($R = 0.73$) and storm duration ($R = 0.48$) were the strongest predictors of dune retreat. In contrast, peak wave direction ($R \approx 0.04$), maximum water level, and initial berm width ($R \approx 0.02$) showed minimal influence. The very weak correlation with berm width suggests that, once storm runup exceeds the dune foot elevation, erosion proceeds largely independent of the pre-storm beach width. While wider berms may delay the onset of erosion, they do not significantly reduce the total volume removed once the dune is actively retreating. This is consistent with findings from Itzkin et al. (2021), who showed that the magnitude of erosion is ultimately governed by storm duration and surge level rather than beach width alone. These results emphasize that sustained wave attack—rather than short-lived peak conditions or spatial buffers—is the dominant control on dune retreat in collision-dominated erosion regimes.

Implications for modeling and coastal management

This study presents a computationally efficient and physically grounded framework capable of resolving both alongshore and cross-shore processes in a barrier island setting. By coupling a one-line shoreline model with an impact-based dune erosion module, and driving it with nearshore wave forcing from SnapWave, the model reproduced observed patterns of shoreline change, dune retreat, and sediment redistribution under storm forcing. The results demonstrate that dune erosion and overwash are integral to short-term and long-term shoreline dynamics and must be explicitly included in predictive models. For coastal managers, the findings underscore the value of preserving dune mobility and sediment connectivity, especially in less-developed areas, while using models like this to identify critical zones for targeted intervention. Future efforts should focus on incorporating dynamic overwash feedbacks, improving remote sensing proxies, and applying this framework to assess resilience under climate-driven shifts in storm regimes.

https://doi.org/10.5194/egusphere-2025-2384
Preprint. Discussion started: 26 June 2025

Appendix A – Offshore wave data corrections using Faro buoy

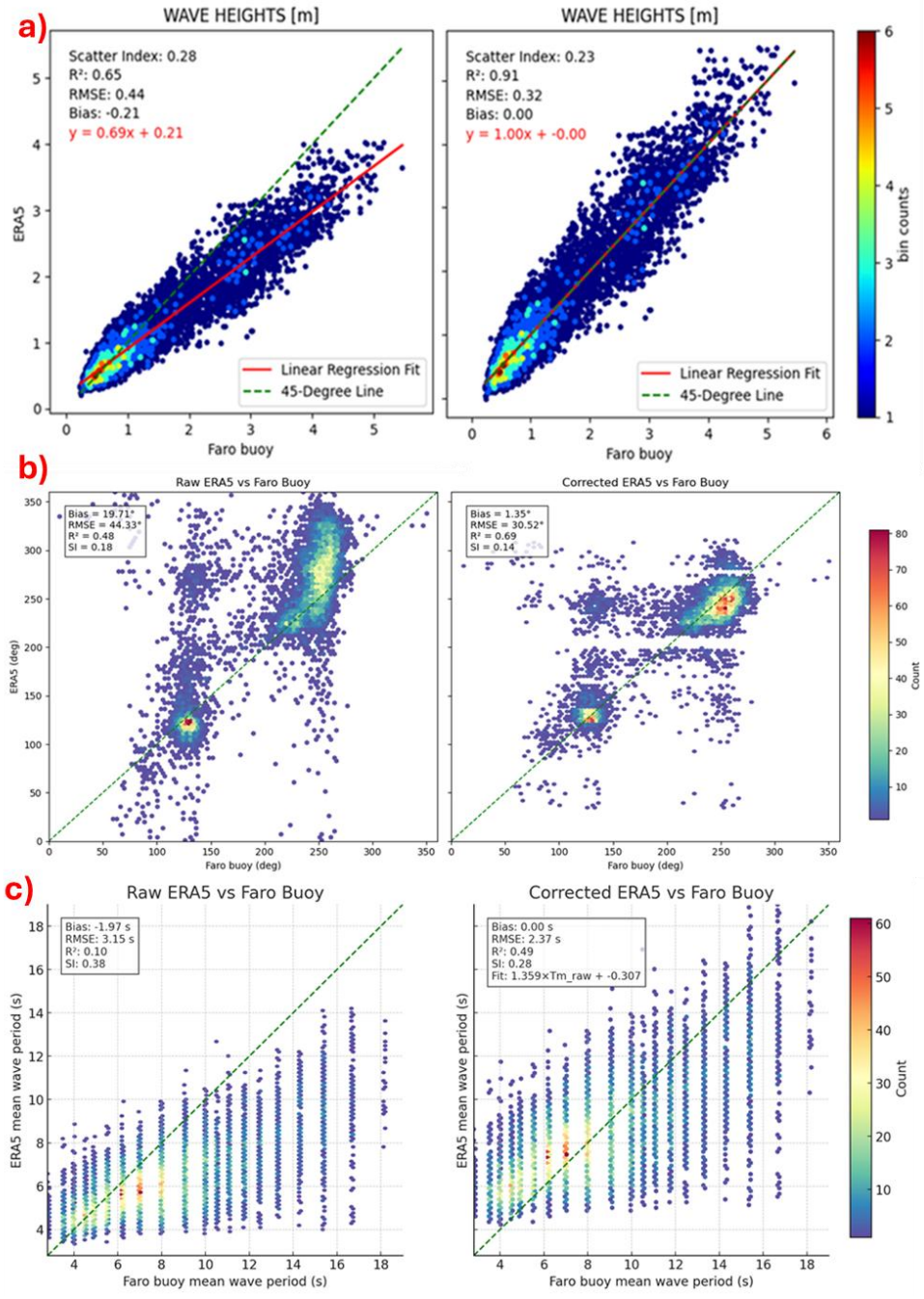

Figure A1. Bias correction of ERA5 wave parameters using Faro buoy data. a) Significant wave height before and after linear correction, with improved correlation and reduced bias. b) Mean wave direction corrected per 30° sector, reducing directional bias and scatter. c) Mean wave period correction improved alignment with buoy data, eliminating bias and reducing RMSE.

https://doi.org/10.5194/egusphere-2025-2384
Preprint. Discussion started: 26 June 2025

670

Figure A2. Locations of ERA5 point vs Faro buoy (© Google Earth)

https://doi.org/10.5194/egusphere-2025-2384
Preprint. Discussion started: 26 June 2025

Figure A3. SnapWave twenty-six model observation points positioned at 400 m offshore along Culatra Island from east to west. These points provide nearshore wave data input for the ShorelineS shoreline evolution model.

https://doi.org/10.5194/egusphere-2025-2384
Preprint. Discussion started: 26 June 2025

Appendix B – Dune Model Calibration: Insights into Cs and d50

We integrated a dune erosion and recovery module based on the impact-based model of Larson et al. (2016), which simulates dune erosion when wave runup exceeds the dune foot and aeolian sand deposition during calm periods. A key parameter in the dune erosion formula is the impact coefficient C_s, a dimensionless factor scaling the efficiency of wave impact in eroding the dune face. Larson et al. (2016) suggest a default $C_s \approx 2.5\times10^{-4}$ for medium sand. We began with this value and conducted sensitivity tests (**Figure B1**). The model showed a linear increase in dune erosion with higher C_s, as expected. To match the observed dune retreat in the central-western "hotspot" (see Section 7) and the observed overwash in the eastern part, we found that a substantially lower C_s (~$7.5\times10^{-}5$) was necessary. This calibrated value (approximately one-third the Larson et al., 2016 default produced dune erosion volumes after the four largest storms that aligned with lidar-estimated losses. The need for a lower C_s may reflect local factors on Culatra: for example, reflective beach conditions or pre-existing dune scarps can make wave impacts more effective at dislodging sand. A similar range of C_s (10^{-5}–10^{-4}) has been used in other impact-based dune erosion studies after site-specific calibration (Palalane et al., 2016)

Figure B1 highlights the model's sensitivity to C_s. The dune foot retreat during storms increases from only a few meters (for $C_s = 7.5\times10^{-6}$) to well over 10 m (for $C_s = 7.5\times10^{-4}$) in the hotspot area. We selected $C_s = 7.5\times10^{-5}$ as the calibrated value that best matched the total volume of dune erosion observed. This calibration exercise underscores that C_s must be site-tuned – small changes can significantly alter erosion predictions. Meanwhile, adjustments to d_{50} confirmed that larger grain sizes yield negligible wind transport (virtually zero dune recovery over the two-year simulation), which aligned the model with observations of persistent dune deficits. In summary, the dune module's performance was highly sensitive to the wave impact coefficient and sediment size. We proceeded with the calibrated values (C_s ~7.5×10^{-3}, d_{50} = 0.5 mm) for subsequent validation and scenario runs.

https://doi.org/10.5194/egusphere-2025-2384
Preprint. Discussion started: 26 June 2025

Figure B1. Sensitivity of dune erosion to variations in the impact coefficient (Cs). Higher Cs values lead to increased dune erosion during storm events.

We also calibrated the aeolian dune recovery component. Larson et al. (2016) treated wind transport with a threshold shear velocity and efficiency factor; in our model, this is implicitly linked to sand grain size and wind speed. Based on regional sediment data (Ferreira et al., 2016) and field judgment, we set the median grain size $d_{50} \approx 0.5$ mm (coarse sand) for the dune and beach. This choice greatly influences wind-blown transport because coarser sand is harder to mobilize. Indeed, using $d_{50} = 0.5$ mm in the model yielded very slow dune growth during inter-storm lulls, consistent with anecdotal observations that the dune foot advanced only modestly seaward during the calm summer of 2010. For a 10 m s^{-1} onshore wind, the modeled transport rate was on the order of 10^{-5} $m^3/m/s$ (comparable to values in Larson et al., 2016 after calibration). If we instead tried finer sand, the model does not change post-storm dune recovery, meaning low wind speeds in the area results in limited dune growth by wind regardless of grain size tried ranging from 0.2 mm to 0.5 mm (**Figure B2**)

https://doi.org/10.5194/egusphere-2025-2384
Preprint. Discussion started: 26 June 2025

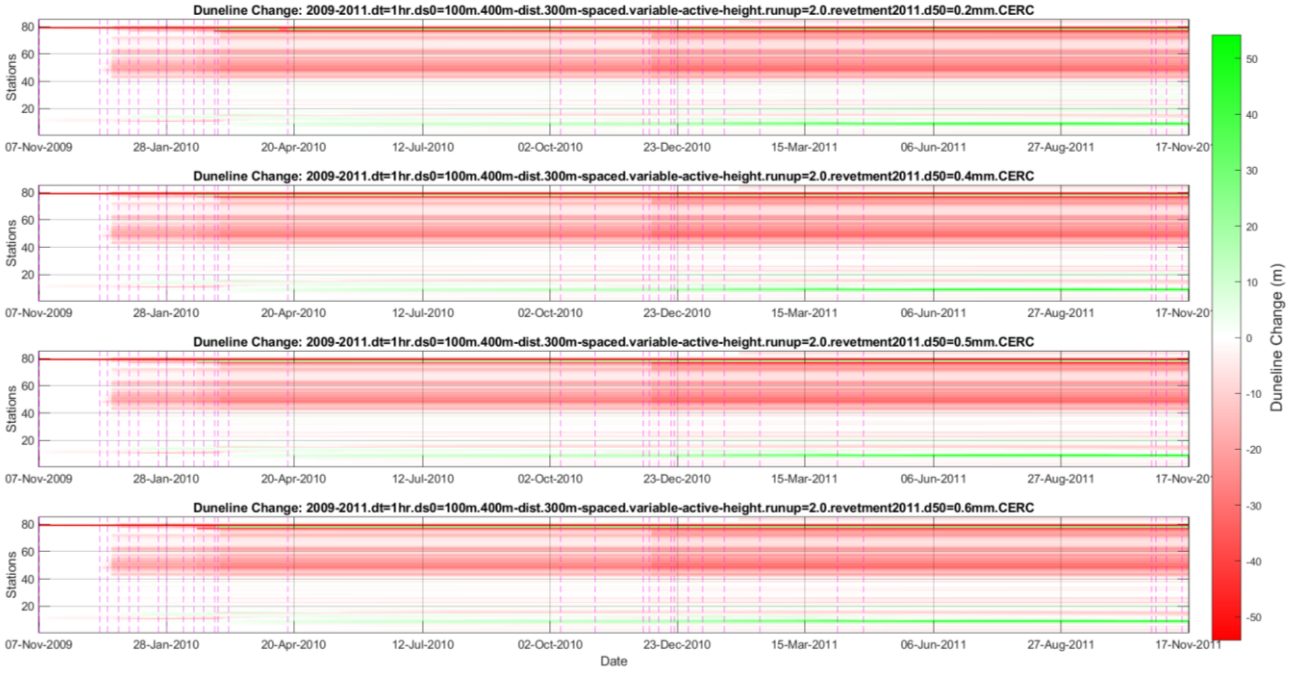

Figure B2. Modeled dune foot position change from 2009 to 2011 under varying sediment grain sizes (d_{50} = 0.2–0.6 mm) across all stations along Culatra Island. Despite the use of smaller sediment sizes that should enhance aeolian transport, limited dune recovery is observed due to persistently low wind speeds. Red shading indicates erosion; green shading indicates accretion. Dashed vertical lines denote the timing of storm events.

Author contribution

R. Dabu applied the coupled shoreline and dune model, performed parameter calibration and model validation, analyzed and interpreted the results, and led the original manuscript writing and visualization.

D. Roelvink conceptualized the experiment, developed the overall modeling approach, and provided supervision and technical guidance. He also reviewed and revised the manuscript.

J. Garzon contributed to data acquisition, processing, and interpretation, and reviewed the manuscript draft.

A. van Dongeren contributed to the study concept, coordinated project administration, and provided strategic input on the research direction.

https://doi.org/10.5194/egusphere-2025-2384
Preprint. Discussion started: 26 June 2025

Acknowledgements

This research was supported by the CoastHazar Erasmus+ Program, which provided funding for the academic mobility and research activities enabling this work. We gratefully acknowledge the Portuguese Environment Agency (APA) and the University of Algarve (UAlg) for providing access to 2009 and 2011 LiDAR datasets. We also acknowledge the Portuguese Instituto Hidrográfico for providing wave buoy information. Satellite imagery was obtained from the Landsat 5, 7, and 8 missions, processed through the CoastSat toolkit (Vos et al., 2019). Wave data used for model forcing were sourced from the Faro buoy and ERA5 reanalysis datasets from ECMWF. Juan L. Garzon was funded by the Portuguese Foundation of Science and Technology (FCT) through UIDP/00350/2020, CEECINST/00146/2018/CP1493/CT0012 and LA/P/0069/2020. Ap van Dongeren was funded through the Deltares Moonshot 2 Program. We are especially thankful to Oscar Ferreira for his valuable support and insights in the analysis of LiDAR data. The authors also thank the members of the ShorelineS and SnapWave development teams, and the reviewers for their constructive feedback that helped improve this manuscript. We thank Bas Huisman for his constructive feedback during the thesis defense, which helped improve the final version of the manuscript.

https://doi.org/10.5194/egusphere-2025-2384
Preprint. Discussion started: 26 June 2025

References

Anthony, E. J.: Patterns of sand spit development and their management implications on deltaic, drift-aligned coasts: The cases of the Senegal and Volta River delta spits, West Africa, in Sand and Gravel Spits (ed. Randazzo et al.), Coastal Research Library, **12**, Springer, pp. 21–45, https://doi.org/10.1007/978-3-319-13716-2_2 , 2015.

Ashton, A. D. and Murray, A. B.: High-angle wave instability and emergent shoreline shapes: 1. Modeling of sand waves, flying spits, and capes, J. Geophys. Res.-Earth Surf., 111, F04011, https://doi.org/10.1029/2005JF000422, 2006.

Bamunawala, J., Ranasinghe, R., and Sirisena, J.: Impact of ebb-delta dynamics on shoreline evolution along inlet-interrupted coasts, Front. Mar. Sci., 10, 1224881, https://doi.org/10.3389/fmars.2023.1224881, 2023.

Beck, T. M. and Wang, P.: Morphodynamics of barrier-inlet systems in the context of regional sediment management, with case studies from west-central Florida, Ocean and Coastal Management, **177**, 31–51, https://doi.org/10.1016/j.ocecoaman.2019.04.022, 2019.

Beuzen, T., Harley, M. D., Splinter, K. D., and Turner, I. L.: Controls of variability in berm and dune storm erosion, J. Geophys. Res.-Earth Surf., 124, 1435–1452, https://doi.org/10.1029/2019JF005184, 2019.

Beuzen, T.: pybeach: A Python package for extracting the location of dune toes on beach profile transects, J. Open Source Softw., 4, 1890, https://doi.org/10.21105/joss.01890, 2019.

Burvingt, O., Masselink, G., Russell, P., and Scott, T.: Classification of beach response to extreme storms, Geomorphology, 295, 722–737, https://doi.org/10.1016/j.geomorph.2017.07.022 , 2017.

Camus, P., Losada, I. J., Izaguirre, C., Espejo, A., Menéndez, M., and Pérez, J.: Statistical wave climate projections for coastal impact assessments, Earth's Future, 5, 918–933, https://doi.org/10.1002/2017EF000609, 2017.

Castelle, B., Masselink, G., Scott, T., Stokes, C., Konstantinou, A., Marieu, V., and Bujan, S.: Satellite-derived shoreline detection at a high-energy meso-macrotidal beach, Geomorphology, 383, 107707, https://doi.org/10.1016/j.geomorph.2021.107707, 2021.

Dissanayake, P., Brown, J., Wisse, P., and Karunarathna, H.: Effects of storm clustering on beach/dune evolution, Mar. Geol., 370, 63–75, https://doi.org/10.1016/j.margeo.2015.10.010, 2015.

Fanti, V., Ferreira, Ó., Kümmerer, V., and Loureiro, C.: Improved estimates of extreme wave conditions in coastal areas from calibrated global reanalyses, Commun. Earth Environ., 4, 151, https://doi.org/10.1038/s43247-023-00819-0, 2023.

Ferreira, Ó., Matias, A., and Pacheco, A.: The east coast of Algarve: A barrier island dominated coast, J. Coast. Res., SI75, 69–73, 2016.

FitzGerald, D. M.: Sediment bypassing at mixed energy tidal inlets, in: Proc. 18th Coastal Engineering Conference, American Society of Civil Engineers, Cape Town, South Africa, 1094–1118, 1982

Garzon, J. L., Costas, S., and Ferreira, Ó.: Biotic and abiotic factors governing dune response to storm events, Earth Surf. Process. Landf., 47, 1013–1031, https://doi.org/10.1002/esp.5300 , 2022.

Herrling, G. and Winter, C.: Tidal inlet sediment bypassing at mixed-energy barrier islands, Coastal Eng., 136, 1–19, https://doi.org/10.1016/j.coastaleng.2018.08.008, 2018.

Hersbach, H., Bell, B., Berrisford, P., Hirahara, S., Horányi, A., Muñoz-Sabater, J., Nicolas, J., Peubey, C., Radu, R., Schepers, D., Simmons, A., Soci, C., Abdalla, S., Abellan, X., Balsamo, G., Bechtold, P., Biavati, G., Bidlot, J., Bonavita, M., De Chiara, G., Dahlgren, P., Dee, D., Diamantakis, M., Dragani, R., Flemming, J., Forbes, R., Fuentes, M., Geer, A., Haimberger, L., Healy, S., Hogan, R. J., Hólm, E., Janisková, M., Keeley, S., Laloyaux, P., Lopez, P., Lupu, C., Radnoti, G., de Rosnay, P., Rozum, I., Vamborg, F., Villaume, S., and Thépaut, J.-N.: The ERA5 global reanalysis, Q. J. Roy. Meteorol. Soc., 146, 1999–2049, https://doi.org/10.1002/qj.3803 , 2020

Houser, C.: Alongshore variation in the morphology of coastal dunes: Implications for storm response, Geomorphology, 199, 48–61, https://doi.org/10.1016/j.geomorph.2012.10.035, 2013

Itzkin, M., Moore, L. J., Ruggiero, P., Hacker, S. D., and Biel, R. G.: The relative influence of dune aspect ratio and beach width on dune erosion as a function of storm duration and surge level, Earth Surf. Dynam., 9, 1223–1237, https://doi.org/10.5194/esurf-9-1223-2021, 2021.

Kombiadou, K., Carrasco, A. R., Costas, S., Ramires, M., and Matias, A.: The birth of backbarrier marshes in Culatra Island (Ria Formosa, South Portugal), Estuar. Coast. Shelf Sci., 296, 108589, https://doi.org/10.1016/j.ecss.2023.108589, 2024.

https://doi.org/10.5194/egusphere-2025-2384
Preprint. Discussion started: 26 June 2025

Kombiadou, K., Matias, A., Ferreira, Ó., Carrasco, A. R., Costas, S., and Plomaritis, T.: Impacts of human interventions on the evolution of the Ria Formosa barrier island system (S. Portugal), Geomorphology, 343, 129–144, https://doi.org/10.1016/j.geomorph.2019.07.006, 2019.

Kümmerer, V., Ferreira, Ó., Fanti, V., and Loureiro, C.: Storm identification for high-energy wave climates as a tool to improve long-term analysis, Clim. Dyn., 62, 2207–2226, https://doi.org/10.1007/s00382-023-07017-w, 2024.

Larson, M., Erikson, L., and Hanson, H.: An analytical model to predict dune erosion due to wave impact, Coast. Eng., 51, 675–696, https://doi.org/10.1016/j.coastaleng.2004.07.003, 2004.

Larson, M., Erikson, L., and Hanson, H.: Modeling runup and overwash based on collision regimes, J. Coast. Res., 25, 835–843, https://doi.org/10.2112/08-1039.1, 2009.

Larson, M., Palalane, J., Fredriksson, C., and Hanson, H.: Simulating cross-shore material exchange at decadal scale: Theory and model component validation, Coast. Eng., 116, 57–66, https://doi.org/10.1016/j.coastaleng.2016.05.009, 2016.

Lettau, K. and Lettau, H.: Experimental and micrometeorological field studies of dune migration, in: Exploring the World's Driest Climate, edited by: Lettau, H. and Lettau, K., IES Report 101, University of Wisconsin–Madison, 110–147, 1978.

Levin, N. and Ben-Dor, E.: Monitoring sand dune stabilization along the coastal dunes of Ashdod–Nizanim, Israel, 1945–1999, J. Arid Environ., 58, 335–355, https://doi.org/10.1016/j.jaridenv.2003.08.007 , 2004.

Masselink, G. and Lazarus, E. D.: Defining coastal resilience, Water, 11, 2587, https://doi.org/10.3390/w11122587, 2019.

Masselink, G., Castelle, B., Scott, T., Dodet, G., Suanez, S., Jackson, D., and Floc'h, F.: Extreme wave activity during 2013/2014 winter and morphological impacts along the Atlantic coast of Europe, Geophys. Res. Lett., 43, 2135–2143, https://doi.org/10.1002/2015GL067492 , 2016a.

Masselink, G., Scott, T., Poate, T., Russell, P., Davidson, M., and Conley, D.: The extreme 2013/2014 winter storms: hydrodynamic forcing and coastal response along the southwest coast of England, Earth Surf. Process. Landf., 41, 378–391, https://doi.org/10.1002/esp.3836, 2016b.

Mortlock, T. R., Goodwin, I. D., McAneney, J. K., and Roche, K.: The June 2016 Australian East Coast Low: Importance of wave direction for coastal erosion assessment, Water, 9, 121, https://doi.org/10.3390/w9020121, 2017.

https://doi.org/10.5194/egusphere-2025-2384
Preprint. Discussion started: 26 June 2025

Muir, F. M. E., Hurst, M. D., Richardson-Foulger, L., Rennie, A. F., and Naylor, L. A.: VedgeSat: An automated, open-source toolkit for coastal change monitoring using satellite-derived vegetation edges, Earth Surf. Process. Landf., 49, 2405–2423, https://doi.org/10.1002/esp.5835, 2024.

Palalane, J., Fredriksson, C., Marinho, B., Larson, M., Hanson, H., and Coelho, C.: Simulating cross-shore material exchange at decadal scale: Model application, Coast. Eng., 116, 26–41, https://doi.org/10.1016/j.coastaleng.2016.05.007, 2016.

Roelvink, D., Huisman, B., Elghandour, A., Ghonim, M., and Reyns, J.: Efficient modeling of complex sandy coastal evolution at monthly to century time scales, Front. Mar. Sci., 7, 535, https://doi.org/10.3389/fmars.2020.00535, 2020.

Roelvink, D., van Ormondt, M., Reyns, J., and van der Lugt, M.: SnapWave: fast, implicit wave transformation from offshore to nearshore, EGUsphere [preprint], https://doi.org/10.5194/egusphere-2025-492, 2025.

Sallenger, A. H.: Storm impact scale for barrier islands, J. Coast. Res., 16, 890–895, 2000.

Stockdon, H. F., Holman, R. A., Howd, P. A., and Sallenger, A. H.: Empirical parameterization of setup, swash, and runup, Coast. Eng., 53, 573–588, https://doi.org/10.1016/j.coastaleng.2005.12.005 , 2006.

Stopa, J. E. and Cheung, K. F.: Intercomparison of wind and wave data from the ECMWF Reanalysis Interim and the NCEP Climate Forecast System Reanalysis, Ocean Model., 75, 65–83, https://doi.org/10.1016/j.ocemod.2013.12.006, 2014.

Vitousek, S., Barnard, P. L., Limber, P., Erikson, L., and Cole, B.: A model integrating longshore and cross-shore processes for predicting long-term shoreline response to climate change, J. Geophys. Res.-Earth Surf., 122, 782–806, https://doi.org/10.1002/2016JF004065 , 2017.

Vos, K., Splinter, K. D., Harley, M. D., Simmons, J. A., and Turner, I. L.: CoastSat: A Google Earth Engine-enabled Python toolkit to extract shorelines from publicly available satellite imagery, Environ. Model. Softw., 122, 104528, https://doi.org/10.1016/j.envsoft.2019.104528, 2019.

Vousdoukas, M. I., Mentaschi, L., Voukouvalas, E., Verlaan, M., Jevrejeva, S., Jackson, L. P., and Feyen, L.: Global probabilistic projections of extreme sea levels show intensification of coastal flood hazard, Nat. Commun., 9, 2360, https://doi.org/10.1038/s41467-018-04692-w, 2018.

https://doi.org/10.5194/egusphere-2025-2384
Preprint. Discussion started: 26 June 2025

Zarnetske, P. L., Hacker, S. D., Seabloom, E. W., Ruggiero, P., Killian, J. R., Maddux, T. B., and Cox, D.: Biophysical feedback mediates effects of invasive grasses on coastal dune shape, Ecology, 93, 1439–1450, https://doi.org/10.1890/11-1112.1 , 2012.